An Investigation into the Maximum Entropy Production Principle in Chaotic Rayleigh-Bénard Convection

R A W Bradford
EDF Energy, Barnett Way, Barnwood, Gloucester, Glos.GL4 3RS, UK
email : rick.bradford@edf-energy.com

Abstract: The hypothesis is made that the temperature and velocity fields in Rayleigh-Bénard convection can be expressed as a superposition of the active modes with time-dependent amplitudes, even in the chaotic regime. The maximum entropy production principle is interpreted as a variational principle in which the amplitudes of the modes are the variational degrees of freedom. For a given Rayleigh number, the maximum heat flow for any set of amplitudes is sought, subject only to the constraints that the energy equation be obeyed and the fluid be incompressible. The additional hypothesis is made that all temporal correlations between modes are zero, so that only the mean-squared amplitudes are optimising variables. The resulting maximal Nusselt number is close to experimental determinations. The Nusselt number would appear to be simply related to the number of active modes, in particular the number of distinct vertical modes. It is significant that reasonable results are obtained for the optimised Nusselt number in that the dynamics (the Navier-Stokes equation) is not used as a constraint. This suggests grounds for optimism that the maximum entropy production principle, interpreted in this variational manner, can provide a reasonable guide to the dynamic steady states of non-equilibrium systems whose detailed dynamics are unknown.

PACS numbers: 47.20.Bp, 47.27.eb
Keywords: Rayleigh-Bénard convection, maximum entropy production, chaotic
Submitted to: *Physica* A

1. Introduction

The existence of general extremal principles in non-equilibrium thermodynamics is contentious. A suggestion which has gained popularity in some quarters is that a non-equilibrium system in a dynamic steady state will maximise its rate of entropy production. This is referred to as the Maximum Entropy Production Principle (MEPP). There is no proof of this hypothesis in the general case, though attempts in this direction have been made, notably by Dewar, [1, 2]. However, whilst a rigorous mathematical proof from more basic physics may not be forthcoming, this does not necessarily prevent the principle being of considerable utility in understanding highly complex systems, see for example Bruers [3], Grinstein and Linsker [4], Dewar [5] and Virgo [6]. The generic situation when modelling very complex systems is that some constraints may be secure, such as conservation of energy, but formulating the dynamical equations in sufficient detail to make the model deterministic is often problematical. Deterministic models of complex systems face a choice between including great detail, in which case the model becomes forbiddingly complicated with many free parameters, or to simplify, in which case there is a danger that the essential behaviour is lost. The role of MEPP is to take the place of the detailed dynamics in such models. The argument is that, provided the essential constraints are imposed, MEPP will provide a good account of the key behaviour of the system without the need for a deterministic dynamical model, see for example Martyushev and Seleznev [7], Martyushev [8], Meysman and Bruers [9], and Niven [10].

In this spirit, the lack of a rigorous physical proof has not prevented application of the principle to

specific systems, especially in the fields of ecology, biology and planetary science. Indeed it was the success of the model as applied to the Earth's atmosphere by Paltridge [11] which did much to stimulate interest in MEPP. Since then, proponents of the hypothesis have pointed to its apparent success in modelling the atmospheres not only of the Earth (Dyke and Kleidon [12]) but also of Titan and Mars (Lorenz, Lunine and Withers [13]). Other apparently successful applications of MEPP have been in rationalising transitions among multiple steady states of oceanic thermohaline circulation (Shimokawa & Ozawa [14]), in the behaviour of the Earth's mantle (Lorenz [15]), and in biological systems. The latter includes the claim that steady-state bacterial photosynthesis operates close to maximum entropy production (Juretic and Zupanovic [16]) and also the claim that the molecular motor ATP synthase has evolved in accordance with MEPP (Dewar, Juretic and Zupanovic [17]). MEPP has also proved successful in fluid flow problems, Niven [18]. Nevertheless, MEPP has remained suspect in the physics community due to lack of theoretical justification. Worse still, it is unclear what exactly the principle asserts in the general case due to an element of choice in what constraints are imposed and what variables are used to perform the optimisation.

In view of the absence of a general proof, the credibility of MEPP may be investigated using specific systems whose true behaviour can be either computed or experimentally determined. A system which has been used for this purpose by some authors is Rayleigh-Bénard convection (RBC). This involves a horizontal enclosure of fluid of uniform depth which is heated from below resulting in heat transfer by combined conduction and convection to its upper surface. For temperature gradients in a certain range, this system produces stable convection patterns such as rolls or hexagonal cells. For larger temperature gradients the fluid motion becomes increasingly chaotic and ultimately turbulent. The behaviour of this system is complex enough for the predictions of MEPP to be non-trivial, whilst also being simple enough to be amenable to both numerical analysis and experimental investigation. The idea is that a successful performance of MEPP in this arena might add to the growing confidence in the principle when applied to more complex systems. Conversely, poor performance would cast doubt on the reliability of the principle. Unfortunately a consensus has not yet emerged as regards the veracity of MEPP when applied to Rayleigh-Bénard systems.

In 1958 Malkus and Veronis [19] proposed the hypothesis that the selected Rayleigh-Bénard convection mode was that with the greatest heat transport. Early doubt that this is so arose from observations that selected modes tend to have wavelengths greater than the critical wavelength, whereas the greatest heat transport is expected for shorter wavelengths, Koschmieder [20]. However, in his analysis of RBC, Kita [21,22] concluded that, "*the system is found to evolve from the heat-conducting uniform state towards the convective roll state with monotonic increase of entropy on the average. Thus, the principle of maximum entropy proposed for non-equilibrium steady states..... is indeed obeyed in this prototype example*." Similarly, Cafaro and Saluzzi [23] concluded that, "*the entropy production rate and the entropy flux increase when convection appears*". These observations are not terribly surprising since the onset of convection is easily seen to increase the heat flux, and, for fixed temperature boundary conditions, this is virtually synonymous with an increased rate of entropy production. However, more recently Weaver, Dyke and Oliver [24] have reported that a lattice Boltzmann model implies that, "*more efficient dissipative convection configurations are universally more stable*". For different system aspect ratios, different convection modes produce the greatest heat flux. By slowly expanding or contracting the system width, Weaver *et al* [24] report that transitions to the highest heat flux mode occur consistently. For boundary conditions approximating to applied fluid temperatures this is equivalent to the selected mode being chosen according to MEPP. In apparent contradiction to this, the analysis by Attard [25,26] results in the conclusion that, "*the calculated spontaneous conduction-convection transition yields a final state that does not correspond to an extremity of the Nusselt number. The present results, as well as earlier results* (Busse [27] and Busse

and Whitehead [28]) *show that the observed convective patterns following a spontaneous transition do not correspond to either the maximum nor to the minimum heat flux. Hence the superficial conclusion from these quantitative observations is that neither the maximum dissipation nor the minimum dissipation yield the optimum non-equilibrium state*." Attard concludes that the final state depends upon the initial state, not just the state of greatest (or least) entropy production.

In short, the present position of MEPP in Rayleigh-Bénard convection is unclear. However, let us suppose that the conclusion of Koschmieder [20] and Attard [25,26] is the right one and that MEPP has apparently been discredited in this context. A proponent of MEPP might claim that the principle has not yet been tested in the correct regime. Indeed, proponents of MEPP do consistently emphasise that the principle will hold only for systems which are "sufficiently complex". But all the investigations of RBC referred to above involve the sub-chaotic regime in which the system is either static or in a stable convection-cell state, or transitions between two such states. This may not be the most appropriate regime in which to investigate extremal principles in RBC. Rather extremal principles may be more appropriate in the chaotic regime. By the same token, the failure of MEPP in the chaotic regime would constitute a more robust refutation. Consequently in this paper we investigate the principle in the chaotic regime (as well as the sub-chaotic regime). To do so it is first necessary to identify the degrees of freedom with respect to which the extremal behaviour is postulated. These are identified here with the time-dependent amplitudes of the marginally stable modes out of which we hypothesise the fluid motion may be regarded as composed.

The paper is organised as follows. Section 2 makes reference to existing lines of investigation into heat transport bounds in RBC and emphasises the very different objectives and methodology of this paper. Section 3 summarises the fluid and energy equations in the Boussinesq approximation and provides a reminder of the linear perturbation solutions for the marginally stable convective states. Section 4 argues that, for our specific purposes, a sufficiently general fluid state can be represented as a linear composition of these marginally stable 'modes' with time-dependent amplitudes. Section 5 formulates the variational principle to be deployed and introduces an equation which constrains the amplitudes of the contributing modes as well as an equation for the Nusselt number in terms of these amplitudes. Section 6 describes how the variational problem is solved numerically and presents the results for the maximal Nusselt number obtained with the method. Section 7 is a reminder of the solution for the Nusselt number for a single pure mode. Section 8 compares our calculated maximal Nusselt numbers with experimental and numerical evaluations. Finally Section 9 discusses the significance of the results.

2. Existing Bounding Approaches Contrasted with this Paper

Because of the difficulty of solving the equations of fluid flow and heat transport in RBC, many workers have been motivated to derive upper bounds to the heat flow instead. This arguably started with the work of Malkus and Veronis [19] and Howard [29] and a summary of the history of this approach can be found in Worthing [30]. Recently improved rigorous upper bounds have been provided by Otto and Seis [31] and Whitehead and Doering [32]. Since these analyses also seek upper bounds to the heat transfer there is a danger of confusing them with the objective of the present paper. The key difference is whether or not the dynamical (Navier-Stokes) equation is used. Analyses such as [19,29-32] use the full equation set, including the Navier-Stokes equation, but derive upper bounds on the heat transfer as an alternative to solving the equations directly.

In contrast, the present paper seeks to treat the RBC system in a manner analogous to those cases where MEPP would be deployed "in earnest": that is, to systems for which the detailed dynamics is prohibitively difficult to represent explicitly as equations. Consequently the novel aspect of the present work is that the dynamical (Navier-Stokes) equation is deliberately not used. Instead it is replaced by

MEPP. To be more precise, appeal to Navier-Stokes is confined to the form of the fields considered, namely as an expansion in terms of the active marginally stable modes. But the amplitudes of each of the modes in the expansion are free variables. The paper seeks to determine the maximum heat transfer with respect to variations in these amplitudes, subject only to the constraint of energy conservation and incompressibility. We wish to discover whether this maximum compares well with true (experimental) rates of heat transfer. It is important to appreciate that, *a priori*, the maximum heat transfer determined without imposing the dynamical Navier-Stokes constraint could be wildly wrong. To anticipate, the fact that our results compare reasonably well with experimental data is a significant finding in favour of the MEPP method.

It is emphasised that this paper does not seek to improve knowledge of the magnitude of heat transfer in RBC. The purpose is to examine the performance of MEPP when the detailed dynamics are not employed as a constraint.

3. The Marginally Stable States in Rayleigh-Bénard Convection

The equations of fluid dynamics are derived in standard texts and are summarised here for completeness only. In common with most sources on Rayleigh-Bénard convection we shall work in the Boussinesq approximation. This is the assumption that the material properties are temperature independent except in the buoyancy term, where the temperature variation of the density drives the buoyancy force and causes the convection. Also in common with usual practice, the viscous dissipation term in the energy equation is neglected. The energy equation is thus,

$$\left(\partial_t + \overline{u}\cdot\overline{\nabla}\right)T = \kappa\nabla^2 T \tag{1}$$

where κ is the thermal diffusivity, $\overline{u}$ the fluid velocity and T its temperature. The equation of motion (Navier-Stokes) is,

$$\left(\partial_t + \overline{u}\cdot\overline{\nabla}\right)\overline{u} = -g\left[1+\alpha\left(T_B - T\right)\right]\hat{z} - \frac{1}{\rho}\overline{\nabla}P + \nu\nabla^2\overline{u} \tag{2}$$

where α is the volumetric coefficient of thermal expansion of the fluid, ρ its average density, ν its kinematic viscosity, T_B the temperature of the bottom layer of fluid, and $\hat{z}$ is the vertically upwards unit vector. To equations (1) and (2) we add the requirement for incompressibility,

$$\overline{\nabla}\cdot\overline{u} = 0 \tag{3}$$

Equations (1), (2) and (3) provide a complete specification of the dynamics of the fluid, given suitable boundary conditions and initial conditions. The static solution, when heat flows by conduction only, is $\overline{u} = 0$ and,

$$T = T_0 = \frac{1}{2}\left(T_B + T_T\right) - \beta z \qquad \text{where,} \quad \beta = \frac{\left(T_B - T_T\right)}{b} = \frac{\Delta T}{b} \tag{4}$$

and $T_T < T_B$ is the temperature of the top layer of fluid and b is the vertical thickness of the fluid. The origin of the z coordinate is on the mid-plane of the fluid.

That convection in horizontal layers of fluid, heated from below, gives rise to regular cellular patterns appears to have first been noted in scientific writing by James Thomson [33]. The first quality experimental investigations into this phenomenon were carried out by Bénard [34, 35]. The theoretical explanation for what later became known as Rayleigh-Bénard convection was published by Lord Rayleigh [36]. This is accomplished by considering the velocity, and the difference of the temperature

field from the static solution, $T_1 = T - T_0$, to be small perturbations. This method of deriving the marginally stable modes is treated in standard texts, e.g., Chandrasekhar [37]. For a steady state in which time derivatives vanish this leads to the linearised equations,

$$T_1 = \theta(z) f(x, y) \tag{5}$$

$$u_x = X(z) \partial_x f \tag{6}$$

$$u_y = X(z) \partial_y f \tag{7}$$

$$u_z = \omega(z) f(x, y) \tag{8}$$

$$\left(\partial_x^2 + \partial_y^2\right) f = -k^2 f \tag{9}$$

$$\left(\partial_z^2 - k^2\right)^3 \omega = -\frac{k^2 R_a}{b^4} \omega \tag{10}$$

$$\theta = \frac{\nu}{\alpha g k^2} \left(\partial_z^2 - k^2\right)^2 \omega \tag{11}$$

$$\left(\partial_z^2 - k^2\right)^2 X = \frac{\alpha g}{\nu} \partial_z \theta \tag{12}$$

where the Rayleigh number is defined in terms of the temperature gradient, β, as follows,

$$R_a = \frac{\alpha \beta g b^4}{\nu \kappa} \tag{13}$$

We shall assume the fluid is confined to a rectangular region with sides $x = 0$, $x = L_x$, $y = 0$ and $y = L_y$ and that the fluid slips freely over these boundaries. Hence, on $x = 0$ and $x = L_x$ the boundary conditions are $u_x = 0$ and $\partial_x^2 u_x = 0$, and on $y = 0$ and $y = L_y$ the boundary conditions are $u_y = 0$ and $\partial_y^2 u_y = 0$. The solutions to Equ.(9) obeying these boundary conditions are,

$$f(x, y) = \cos a_n x \cdot \cos d_p y \tag{14}$$

where, $$a_n = \frac{n\pi}{L_x},\ d_p = \frac{p\pi}{L_y} \quad \text{and} \quad k^2 = a_n^2 + d_p^2 \tag{15}$$

and where $n, p = 0,1,2,3....$ can be any positive integers, or zero, except that n and p may not both be zero. (The case $n = p = 0$ is the static pure conduction solution with no convection). Actually the boundary conditions on the vertical surfaces are rather unphysical in that a fluid contained by rigid boundaries will develop shear stresses due to viscosity. Provided that the size of the container, L_x, L_y, is sufficiently large, however, we may expect the effect of these boundaries to be slight. The assumption of stress-free vertical boundaries simplifies the analysis.

In contrast, the fluid is assumed to be confined between rigid plates at its top and bottom surfaces, $z = b/2$ and $z = -b/2$, and it is essential to model the effects of viscosity at these boundaries if contact is to be made with experimental results obtained from such apparatus. The rigid boundaries will cause all the velocity components to be zero on these surfaces. For an incompressible

fluid the velocity boundary conditions on $z = \pm b/2$ are therefore $\omega = 0$ and $\partial_z \omega = 0$. There are two families of solutions to Equ.(10), either even or odd as functions of z, which may be written,

Even: $$\omega = \cos q_0 z + A \cosh qz + A^* \cosh q^* z \tag{16}$$

Odd: $$\omega = \sin q_0 z + A \sinh qz + A^* \sinh q^* z \tag{17}$$

(These are written as dimensionless, it being understood that they will ultimately be multiplied by an amplitude which will carry the units of velocity). Here q_0 and the complex quantity $q = q_1 + iq_2$ are given by,

$$q_0 = k\sqrt{\tau - 1} \tag{18}$$

$$q_1 = k\sqrt{\frac{(1+\tau/2) + \sqrt{1+\tau+\tau^2}}{2}} \tag{19}$$

$$q_2 = k\sqrt{\frac{-(1+\tau/2) + \sqrt{1+\tau+\tau^2}}{2}} \tag{20}$$

where the quantity τ is, $$\tau = \left(\frac{R_a}{(kb)^4}\right)^{1/3} \tag{21a}$$

In order to respect the boundary conditions, the quantities q_0, q_1, q_2 must obey,

(Even Solutions) $$\frac{\left(q_1 + \sqrt{3}q_2\right)\sinh q_1 + \left(\sqrt{3}q_1 - q_2\right)\sin q_2}{\cosh q_1 + \cos q_2} = -q_0 \tan\frac{q_0}{2} \tag{22}$$

(Odd Solutions) $$\frac{\left(q_1 + \sqrt{3}q_2\right)\sinh q_1 - \left(\sqrt{3}q_1 - q_2\right)\sin q_2}{\cosh q_1 - \cos q_2} = q_0 \cot\frac{q_0}{2} \tag{23}$$

Equations (22) or (23) should be considered as constraining the possible values of τ, since all three of q_0, q_1, q_2 are specified explicitly in terms of τ by (18-20) for a given horizontal wavenumber, k. On the other hand τ is also specified in terms of the Rayleigh number by (21a). Hence (16,17) are solutions of (10) only when the Rayleigh number takes one of the discrete set of 'critical' values, R_c, determined by (22) and (23). Consequently the quantity τ is hereafter understood to be one of the discrete set of values,

$$\tau = \left(\frac{R_c}{(kb)^4}\right)^{1/3} \tag{21b}$$

Equs.(16) or (17) then give the solution for the vertical component of velocity via (8). The horizontal components of velocity follow from (6,7) noting that (11,12) imply that $X = \partial_z \omega / k^2$. Finally, the solution for the temperature perturbation, T_1, is given in terms of the solution for ω by (11), giving,

(Even Solutions) $$\widetilde{\theta}(z) = \cos q_0 z - A\xi^* \cosh qz - A^* \xi \cosh q^* z \tag{24}$$

(Odd Solutions) $$\widetilde{\theta}(z) = \sin q_0 z - A\xi^* \sinh qz - A^* \xi \sinh q^* z \tag{25}$$

where, $\xi = \frac{1}{2}\left(1 + i\sqrt{3}\right)$, i.e., $\xi^3 = -1$ (26)

and, $\theta = \frac{\nu\tau^2 k^2}{\alpha g}\widetilde{\theta}$ (27)

The complex amplitude A is found from the boundary conditions $\omega = 0, \partial_z \omega = 0$ and $\theta = 0$ on the top and bottom surfaces. A mode is unstable and will decay exponentially if the Rayleigh number is less than its critical Rayleigh number, R_c. Moreover, these marginally stable solutions should in theory be valid only when R_a exceeds R_c infinitesimally. However, in practice the corresponding mode persists over a reasonable range of Rayleigh number, rendering them experimentally accessible.

For any given horizontal wavenumber, kb, there is an infinite family of solutions for τ, and hence R_c, for each of (22) and (23). These solutions may be labelled by a positive integer $m = 1,2,3...$ in order of increasing critical Rayleigh number, R_c. For $m = 1$, $m = 2$ and $m = 3$ the critical Rayleigh numbers are plotted against the horizontal wavenumber, kb, in Figure 1 (even modes) and Figure 2 (odd modes), and similarly Figures 3 and 4 plot the first 31 modes. The minimum R_c is 1707.762 and occurs for even mode $m = 1$ when kb = 3.117. The minimum R_c for any odd mode is 17,610.55 and occurs for $m = 1$ when kb = 5.3672. Any one of the marginally stable modes can be uniquely identified by four indices: the three mode numbers, n, p, m, plus the parity, i.e., whether an even or an odd solution. The number of active modes (i.e., modes with $R_c < R_a$) increases rapidly with increasing R_a. It also increases with increasing aspect ratio L_x / b and L_y / b. For $R_a = 10^9$ and a square enclosure of aspect ratio 9 there are 5,360,202 active modes.

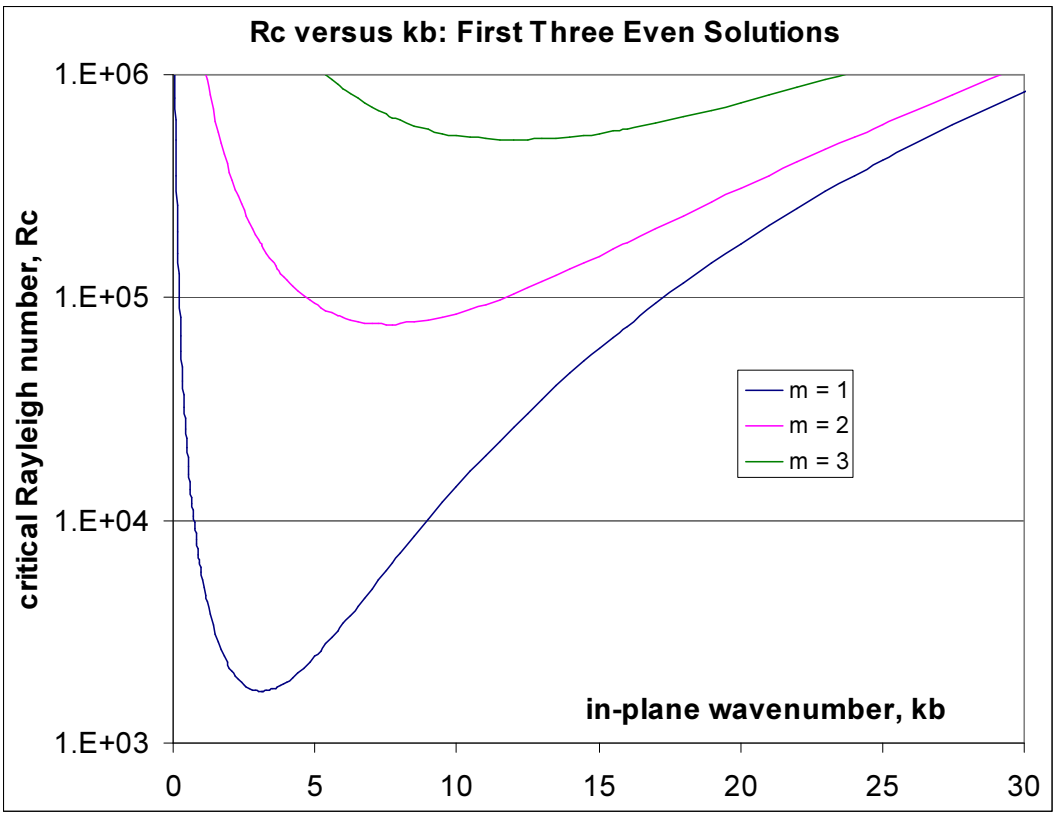

FIG. 1. The first 3 critical Rayleigh numbers for even modes plotted against horizontal wavenumber, kb

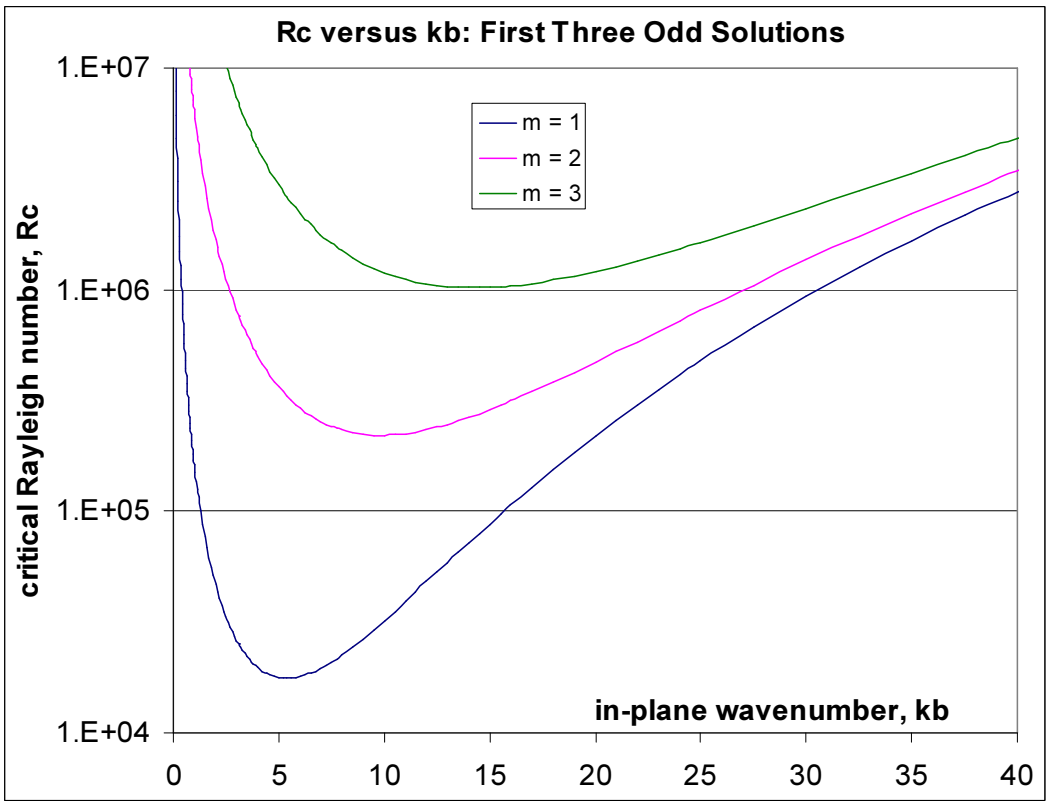

FIG. 2. The first 3 critical Rayleigh numbers for odd modes plotted against horizontal wavenumber, kb

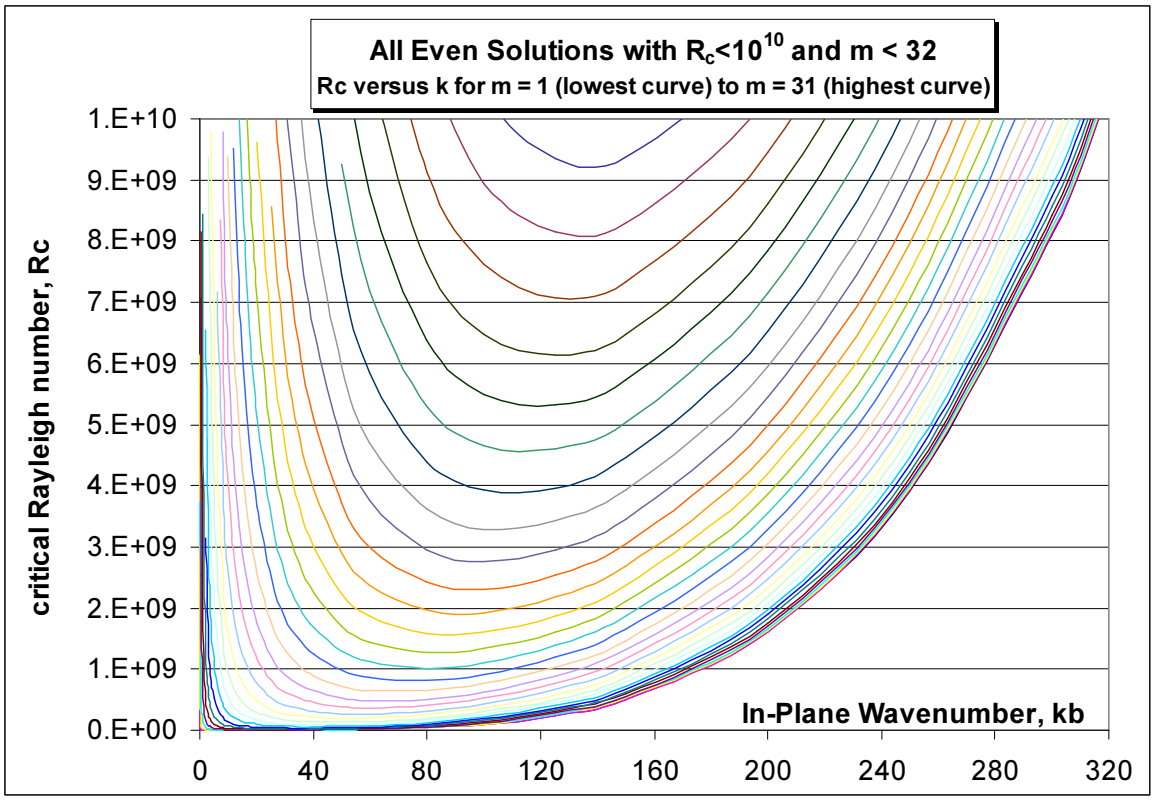

FIG. 3. The first 31 critical Rayleigh numbers for even modes plotted against horizontal wavenumber, kb

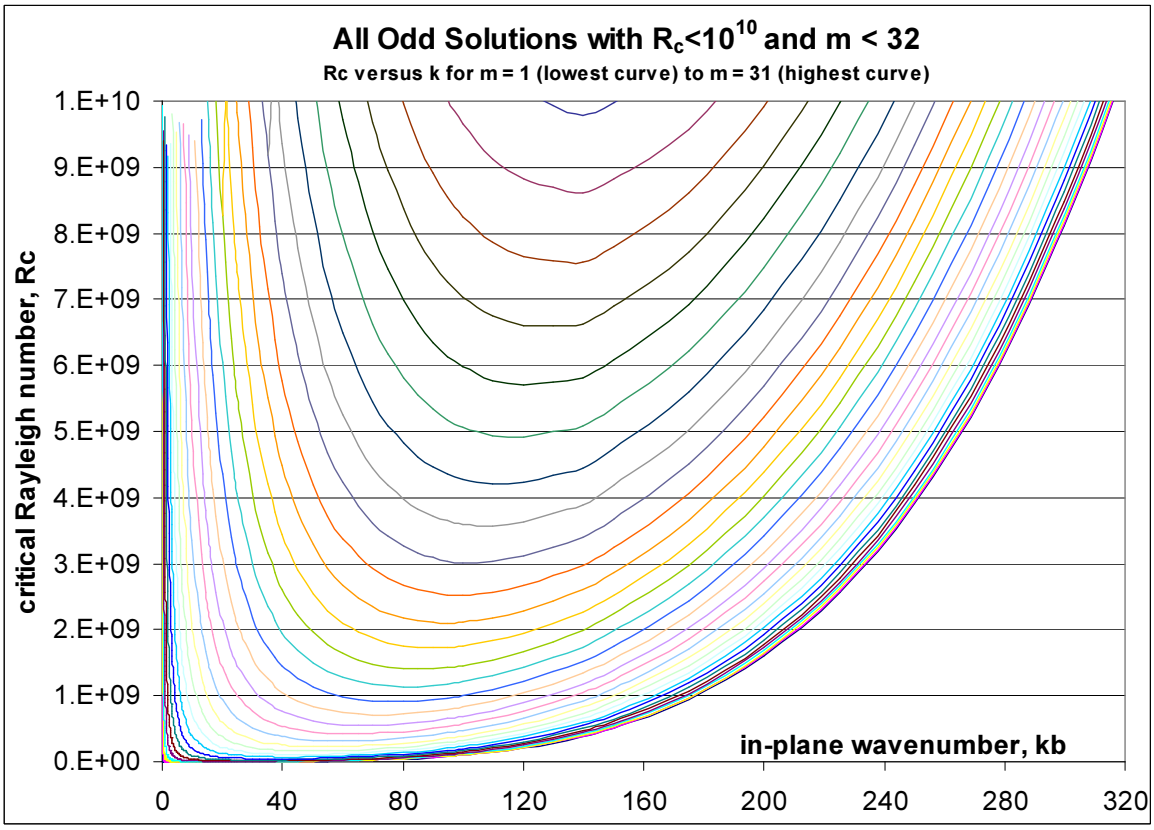

FIG. 4. The first 31 critical Rayleigh numbers for odd modes plotted against horizontal wavenumber, kb

4. The Chaotic Regime

As the Rayleigh number is increased the qualitative nature of the fluid motions undergoes a sequence of transitions. Static, pure conduction first gives way to stable 2D convection rolls when the lowest critical Rayleigh number is exceeded, then to stable 3D convection cells. At larger R_a these stable, time-independent steady states give way to time-dependent chaotic flows of various sorts, and ultimately to fully turbulent conditions at sufficiently high Rayleigh number. The magnitude of R_a at which these transitions occur is dependent upon Prandtl number ($P_r = \nu / \kappa$) , with larger Rayleigh numbers being required to cause the transitions at larger P_r. For water at around room temperature ($P_r \sim 7$) chaotic motion occurs above a Rayleigh number of perhaps $\sim 3\times 10^4$ with turbulence above perhaps $\sim 10^5$ (see Krishnamurti [38]). For $P_r < 1$ (gases, liquid metals) chaotic and turbulent motion may occur at much smaller Rayleigh numbers.

Because the solutions are chaotic for larger Rayleigh numbers, they have no closed form expression. However, consider the following superposition of modal solutions.

$$u_x = -\sum_{npm\chi} a_n \Omega^{\chi}_{npm} X^{\chi}_{npm}(z) \sin a_n x \cdot \cos d_p y \tag{28}$$

$$u_y = -\sum_{npm\chi} d_p \Omega^{\chi}_{npm} X^{\chi}_{npm}(z) \cos a_n x \cdot \sin d_p y \tag{29}$$

$$u_z = \sum_{npm\chi} \Omega^{\chi}_{npm} \omega^{\chi}_{npm}(z) \cos a_n x \cdot \cos d_p y \tag{30}$$

$$T = \widetilde{T}_0 + T_1 \tag{31}$$

$$T_1 = \sum_{npm\chi} \Omega^{\chi}_{npm} \theta^{\chi}_{npm}(z) \cos a_n x \cdot \cos d_p y \tag{32}$$

In these expressions, n, p, m are the mode numbers defined in Section 2, and χ labels the even or odd solutions. The sums in (28-32) extend over the active modes only. Writing the critical Rayleigh numbers as R^{χ}_{npm} , the sums are therefore confined to modes with $R^{\chi}_{npm} < R_a$.

If the amplitudes Ω^{χ}_{npm} were constants, and if $\widetilde{T}_0$ were identified with T_0 , the static solution given by (4), then each term in the above sums would be one of the marginally stable modes. If the underlying equations, (1), (2) and (3) were linear, then (28-32) would simply be the general solution obtained by linear superposition. But, of course, equations, (1), (2) and (3) are not linear and (28-32) are to be understood in a different way. Note that, if Ω^{χ}_{npm} were constants, (28-32) could not even be regarded as an approximate solution in general, because each term is valid only if the corresponding critical Rayleigh number, R^{χ}_{npm} , is just slightly smaller than R_a . But the values of R^{χ}_{npm} for the different active modes may differ by many orders of magnitude (see Figures 1-4), so that this requirement cannot be met for all active modes simultaneously.

The first refinement in the understanding of (28-32) is in regard to $\widetilde{T}_0$. Let us introduce the notation

$\langle ... \rangle_\xi$ to mean averaging over the coordinate ξ, such as,

$$\langle f \rangle_t \equiv \frac{1}{t - t_1} \int_{t_1}^{t} f \cdot dt \tag{33}$$

and,

$$\langle f \rangle_z \equiv \frac{1}{b} \int_{-b/2}^{+b/2} f \cdot dz \tag{34}$$

and,

$$\langle f \rangle_{xy} \equiv \frac{1}{L_x L_y} \int_0^{L_x} \int_0^{L_y} f \cdot dx dy \tag{35}$$

Averaging will be combined in the obvious way, i.e., $\langle f \rangle_{xyz} \equiv \left\langle \langle f \rangle_{xy} \right\rangle_z \equiv \left\langle \langle f \rangle_z \right\rangle_{xy}$, etc. The term $\widetilde{T}_0$ is simply identified with the average temperature over a horizontal plane,

$$\widetilde{T}_0 \equiv \langle T \rangle_{xy} \tag{36}$$

The term T_1 is defined as $T_1 \equiv T - \langle T \rangle_{xy}$ and hence has zero average over any horizontal plane, a property clearly respected by the form of (32). Note, however, that $\widetilde{T}_0$ cannot be simply the linear temperature gradient that prevails in the purely conducting solution, (4), because the heat flux in the vertical direction is given by $-K\partial_z T$ and the contribution of the term T_1 to this averages to zero over the horizontal plane, by definition. Hence the average heat flux due to conduction is simply $-K\left\langle \partial_z \widetilde{T}_0 \right\rangle_{xyt}$. Moreover, if this is evaluated on $z = \pm b/2$ this must equal the *total* heat flux through the fluid since the vertical heat flux by convection must be zero at these boundaries. So if $\widetilde{T}_0$ were identified with T_0 this would imply that convection causes no increase in the heat flow – a clearly incorrect conclusion. In fact we can write $\widetilde{T}_0 = T_0 + T_2$ and identify $-K\partial_z T_2$ evaluated at $z = \pm b/2$ as the additional heat flux due to the occurrence of convection, and $\langle T_2 \rangle_{xyt}$ must be non-zero at some z values when convection occurs.

The second refinement in the understanding of (28-32) is that the amplitudes Ω_{npm}^{χ} must be regarded as functions of time rather than constants. Note that as regards their spatial dependence, Equs.(28-32) are essentially just a way of writing a rather general spatial function, akin to a Fourier expansion but with the basis functions chosen to respect the required boundary conditions. Permitting the Ω_{npm}^{χ} to be arbitrary functions of time therefore allows (28-32) to be understood as merely a convenient representation of an "almost arbitrary" space-time function restricted only by the boundary conditions. The reader will note that the flaw in this reasoning is that (28-32) involve only a finite set of spatial basis functions, which cannot strictly be complete. Moreover, this basis set is smaller at smaller Rayleigh numbers since only active modes are included. Hence, only wavelengths above and below certain limits contribute to (28-32). As regards the horizontal modes, this will be justified *post-hoc*. It will turn out that the optimisation of the heat flow will be accomplished by retaining only those modes whose critical Rayleigh number is not too different from the minimum R_{npm}^{χ} for the relevant χ, m. Consequently even if each χ, m in (28-32) were augmented with larger and smaller horizontal wavenumbers, k, the amplitudes of these extra terms would ultimately be optimised to zero in any

case. In contrast, the restriction of the representation (28-32) to embrace only the 'active' vertical modes, i.e., χ, m values, is an assumption which is significant in determining the optimised Nusselt numbers. For now we let this stand as a declared physical hypothesis, its mathematical status being unclear. However, we speculate upon a possible mathematical origin later (Section 8). Accepting for now that the spatial dependencies of (28-32) are sufficiently general, the temporal dependence is unquestionably so since it is arbitrary.

Chaotic motions are characterised by the absence of periodicity and hence retain time dependence indefinitely. The "steady state" is then defined in terms of suitably time-averaged quantities, i.e.,

$$\frac{\partial}{\partial t}\left\langle T\right\rangle_t = 0 \qquad \text{and} \qquad \frac{\partial}{\partial t}\left\langle u^2\right\rangle_t = 0 \tag{37}$$

5. Formulation of the Extremal Problem Considered

The objective is to find the maximum heat flux which can be achieved with arbitrary amplitudes Ω^{χ}_{npm} subject to the constraint of the energy equation, (1), and the requirement that the fields be of the form of (28-32). The Navier-Stokes equation, (2), is ignored, thus providing the freedom to vary the amplitudes, Ω^{χ}_{npm}, which would otherwise be determined by the dynamics. It is not immediately obvious that the heat flux is even bounded under these conditions. That there *is* a finite upper bound results from the convective derivative in the energy equation, (1). The energy equation together with incompressibility can be used to derive an integral relation which explicitly constrains the magnitude of the amplitudes in (28-32). This integral relation was first derived by Chandrasekhar [37] for the case of strictly stationary states. However a similar relation can be derived for a stochastic, time-averaged, chaotic steady state. In this case it becomes,

$$\beta\left\langle u_z T_1\right\rangle_{txyz} + \kappa\left\langle T_1\nabla^2 T_1\right\rangle_{txyz} = \frac{1}{\kappa}\left\langle\left(\left\langle u_z T_1\right\rangle_{xy}\right)^2\right\rangle_{tz} - \frac{1}{\kappa}\left\langle\left(\left\langle u_z T_1\right\rangle_{xyz}\right)^2\right\rangle_{t} \tag{38}$$

A most important fact is that (38), which is the cornerstone of the optimisation used herein, is quite independent of the Navier-Stokes equation, i.e., it applies independently of the dynamics. This is so important that the full derivation of (38) is presented in the Appendix. Note that the two terms on the RHS differ only in respect of the order in which the square and the z-averaging are carried out. The Nusselt number is shown in the Appendix to be given by,

$$Nu \equiv \frac{\left\langle J\right\rangle_{xyt}}{K\beta} = 1 + \frac{1}{\kappa\beta}\left\langle u_z T_1\right\rangle_{txyz} \tag{39}$$

where $\left\langle J\right\rangle_{xyt}$ is the heat flux averaged over any horizontal plane and over time, and $K = \kappa C\rho$ is the thermal conductivity of the fluid. Note that (38) and (39) involve only the vertical component of velocity, u_z, and the component T_1 of the temperature field which has zero average over horizontal planes. These are given by equations (30) and (32) respectively, the functions ω and θ of the z coordinate being given by (16,17) and (24-27) respectively. Substituting (30) and (32) into (38) or (39) and carrying out the spatial integrals gives expressions which are mode-sums of time-averages of products of the amplitudes, Ω^{χ}_{npm}. It is convenient to absorb a factor of $k\tau$ into the amplitudes,

$$\widetilde{\Omega}^{\chi}_{npm} = k\tau\Omega^{\chi}_{npm} \tag{40}$$

The functions ω^{χ}_{npm} and $\theta^{\chi'}_{npm'}$ are orthogonal in the sense that,

$$\left\langle \omega^{\chi}_{npm}\widetilde{\theta}^{\chi'}_{npm'} \right\rangle_z = \mu^{\chi}_{npm}\delta^{\chi\chi'}\delta_{mm'} \tag{41}$$

which defines the quantities μ^{χ}_{npm}. The functions of x, y in (30) and (32) are also orthogonal for differing n or p. Exploiting these properties (39) becomes,

$$Nu = 1 + \frac{1}{R_a}\left(\frac{b^2}{2\kappa}\right)^2 S1 \tag{42}$$

where,

$$S1 = \sum_{npm\chi} \left\langle \left(\widetilde{\Omega}^{\chi}_{npm}\right)^2 \right\rangle_t \mu^{\chi}_{npm} \tag{43}$$

Substitution of (30) and (32) gives the constraint equation (38) in the form,

$$R_a\left(\frac{2\kappa}{b^2}\right)^2 (S1 - S2) = S3 - S4 \tag{44}$$

where,

$$S2 = \sum_{npm\chi} \left\langle \left(\widetilde{\Omega}^{\chi}_{npm}\right)^2 \right\rangle_t \mu^{\chi}_{npm} \frac{R^{\chi}_{npm}}{R_a} \tag{45}$$

$$S3 = \sum_{npm\chi}\sum_{m'\chi'}\sum_{\widetilde{n}\widetilde{p}\widetilde{m}\widetilde{\chi}}\sum_{\widetilde{m}'\widetilde{\chi}'} \left\langle \widetilde{\Omega}^{\chi}_{npm}\widetilde{\Omega}^{\chi'}_{npm'}\widetilde{\Omega}^{\widetilde{\chi}}_{\widetilde{n}\widetilde{p}\widetilde{m}}\widetilde{\Omega}^{\widetilde{\chi}'}_{\widetilde{n}\widetilde{p}\widetilde{m}'} \right\rangle_t \frac{\tau'\widetilde{\tau}'}{\tau\widetilde{\tau}} \left\langle \omega^{\chi}_{npm}\widetilde{\theta}^{\chi'}_{npm'}\omega^{\widetilde{\chi}}_{\widetilde{n}\widetilde{p}\widetilde{m}}\widetilde{\theta}^{\widetilde{\chi}'}_{\widetilde{n}\widetilde{p}\widetilde{m}'} \right\rangle_z \tag{46}$$

$$S4 = \sum_{npm\chi}\sum_{n'p'm'\chi'} \left\langle \left(\widetilde{\Omega}^{\chi}_{npm}\right)^2 \left(\widetilde{\Omega}^{\chi'}_{n'p'm'}\right)^2 \right\rangle_t \mu^{\chi}_{npm}\mu^{\chi'}_{n'p'm'} \tag{47}$$

where the Rayleigh number, R_a, is defined by (13) and the critical Rayleigh numbers, R^{χ}_{npm}, are derived for each mode in the manner described in Section 2 and plotted in Figures 1-4. In (46) the different τ terms relate to different modes as follows: $\tau \rightarrow npm\chi$; $\tau' \rightarrow npm'\chi'$; $\widetilde{\tau} \rightarrow \widetilde{n}\widetilde{p}\widetilde{m}\widetilde{\chi}$; $\widetilde{\tau}' \rightarrow \widetilde{n}\widetilde{p}\widetilde{m}'\widetilde{\chi}'$. We can now see how (44) constrains the magnitude of the amplitudes (and hence ensures a finite upper bound for the heat flux) since its LHS is quadratic in the amplitudes whereas its RHS is quartic.

Our task is to find the maximum of (42) with respect to variations in the amplitudes, $\widetilde{\Omega}^{\chi}_{npm}$, subject to the constraint (44), where $S1, S2, S3, S4$ are given in terms of the amplitudes by (43,45-47). However, the question of correlations between amplitudes of different modes now arises because (46) and (47) depend upon time averages of products of amplitudes of different modes. It can be shown that if we assume complete freedom to contrive these correlations to maximise the Nusselt number then the result is wildly too large compared with experimental values. However we shall assume no correlation between modes. For example, this means that,

$$\left\langle \left(\widetilde{\Omega}^{\chi}_{npm}\right)^2 \left(\widetilde{\Omega}^{\widetilde{\chi}}_{\widetilde{n}\widetilde{p}\widetilde{m}}\right)^2 \right\rangle_t = \left\langle \left(\widetilde{\Omega}^{\chi}_{npm}\right)^2 \right\rangle_t \left\langle \left(\widetilde{\Omega}^{\widetilde{\chi}}_{\widetilde{n}\widetilde{p}\widetilde{m}}\right)^2 \right\rangle_t \tag{48}$$

The optimisation problem can now be formulated entirely in terms of the mean-squared amplitudes,

$\left\langle \left(\widetilde{\Omega}^{\chi}_{npm}\right)^2 \right\rangle_t$. This optimisation problem can be more succinctly expressed in matrix notation. Define a vector of mean-squared amplitudes by,

$$\bar{f} = \frac{1}{R_a}\left(\frac{b^2}{2\kappa}\right)^2 \left\langle \left(\widetilde{\Omega}^{\chi}_{npm}\right)^2 \right\rangle_t \tag{49}$$

where the vector index corresponds to the mode number in some specified sequence. Similarly defining the vectors,

$$\overline{H} = \mu^{\chi}_{npm} \qquad \text{and} \qquad \overline{h} = \mu^{\chi}_{npm}\left(1 - \frac{R^{\chi}_{npm}}{R_a}\right) \tag{50}$$

the Nusselt number becomes, by re-writing (42,43),

$$Nu = 1 + \overline{H}\cdot\bar{f} \tag{51}$$

whilst the constraint equation (44) becomes, using (43,45-47),

$$\overline{h}\cdot\bar{f} = \bar{f}^T(M)\bar{f} \tag{52}$$

where the matrix (M) follows from (46), having components,

$$\begin{aligned}(M) = &\left[\left\langle \omega^{\chi}_{npm}\widetilde{\theta}^{\chi}_{npm}\omega^{\tilde{\chi}}_{\tilde{n}\tilde{p}\tilde{m}}\widetilde{\theta}^{\tilde{\chi}}_{\tilde{n}\tilde{p}\tilde{m}}\right\rangle_z - \mu^{\chi}_{npm}\mu^{\tilde{\chi}}_{\tilde{n}\tilde{p}\tilde{m}}\right]\Diamond^{\tilde{n}\tilde{p}\tilde{m}\tilde{\chi}}_{npm\chi} + \left(\frac{\tilde{\tau}}{\tau}\right)^2\left\langle \left(\omega^{\chi}_{npm}\widetilde{\theta}^{\tilde{\chi}}_{np\tilde{m}}\right)^2\right\rangle_z \Diamond^{\tilde{m}\tilde{\chi}}_{m\chi}\delta_{n\tilde{n}}\delta_{p\tilde{p}} \\ &+\left\langle \omega^{\chi}_{npm}\widetilde{\theta}^{\chi}_{npm}\omega^{\tilde{\chi}}_{np\tilde{m}}\widetilde{\theta}^{\tilde{\chi}}_{np\tilde{m}}\right\rangle_z \Diamond^{\tilde{m}\tilde{\chi}}_{m\chi}\delta_{n\tilde{n}}\delta_{p\tilde{p}} + \left[\left\langle \left(\omega^{\chi}_{npm}\widetilde{\theta}^{\chi}_{npm}\right)^2\right\rangle_z - \left(\mu^{\chi}_{npm}\right)^2\right]\delta_{n\tilde{n}}\delta_{p\tilde{p}}\delta_{m\tilde{m}}\delta^{\chi\tilde{\chi}}\end{aligned} \tag{53}$$

Here we have introduced the symbol,

$$\Diamond^{xyz\ldots}_{abc\ldots} \equiv \left(1 - \delta^x_a\delta^y_b\delta^z_c\ldots\right) \tag{54}$$

which is 1 unless all of $abc\ldots$ are equal to the corresponding $xyz\ldots$, in which case it is zero.

Hence our variational problem is to maximise Nu, given by (51), with respect to variations in $\bar{f}$ subject to the constraint given by (52), and where $\overline{H}, \overline{h}, M$ are defined in terms of the marginally stable modes by (50) and (53).

A limitation is immediately apparent. Because we are ignoring the dynamics, equation (2), there is no place for the Prandtl number to enter the above extremal problem: equations (50-53) are independent of P_r. Since experimental evaluations of Nu do depend upon P_r there will be an ambiguity regarding which experimental values of Nu are most relevant to compare.

6. Numerical Optimisation

The obvious procedure is to set the derivatives of $1 + \overline{H}\cdot\bar{f} + \lambda\left(\overline{h}\cdot\bar{f} - \bar{f}^T(M)\bar{f}\right)$ to zero, where λ is a Lagrange multiplier. This results in a simple linear equation for $\bar{f}$ in terms of λ, and the latter is then found by imposing (52). But this approach fails because many of the resulting components of $\bar{f}$ are negative, an unphysical outcome because the components of $\bar{f}$ are intended to be mean-squared

amplitudes. The required optimum must enforce all components of $\bar{f}$ to be positive or zero. The outcome of the naive approach suggests that some of the optimised amplitudes will in fact be zero.

The method of steepest ascents was adopted for the optimisation. A maximum of Nu was sought along a line in the direction of the gradient, $\overline{\nabla}_f N_u$, of Nu in f space. If points explored along this line had negative values for some components of f these were replaced by zero. When the line-maximum had been found, the gradient was then re-calculated and the process repeated until further increases in Nu became negligible. Both the gradient and the value of Nu were calculated subject to the constraint of remaining on the surface in f space defined by the constraint equation (52). Such non-linear optimisation techniques are not guaranteed to identify the global maximum. However the fact that the present problem is only quadratic gives some confidence that the global maximum will be found in this case. In fact the process proved robust; widely differing starting amplitudes (i.e., positions in f space) converging to the same optimised Nu. Starting with all components of f equal was sufficient.

An example of the optimised squared-amplitudes obtained for $R_a = 10^5$, $L_x = L_y = 6b$, is shown in Figure 5. The unique mode number used as the abscissa in Figure 5 is defined by listing the active $npm\chi$ sequentially, increasing the left-most first. Hence each of the spikes in Figure 5 gives the squared-amplitudes for the range of n values for a given fixed $pm\chi$. The three separate groups of spikes correspond to: even modes with $m = 1$, even modes with $m = 2$, and odd modes with $m = 1$ respectively (there are no modes with higher m in this case). The individual spikes within any group correspond to different p values.

Figure 5 is typical of the results at other Raleigh numbers and aspect ratios. Most amplitudes are optimised to zero. For a given $m\chi$, the optimisation process tends to leave non-zero amplitudes only for modes with critical Rayleigh numbers close to the minimum for that $m\chi$. This is easy to understand from (52) which will lead to the greatest amplitudes for large $\bar{h}$. But in (50) the factor of $1 - R^{\chi}_{npm} / R_a$ will favour modes with $R^{\chi}_{npm} << R_a$ if the objective is to maximise Nu. This results in np values giving large R^{χ}_{npm} being optimised to zero amplitudes, causing the spikes in Figure 5.

Within any group of spikes, i.e., for a given $m\chi$, the height of the spikes tends to be equal. This is partly because the spikes correspond to different p values and the same, or almost the same, k, and hence R^{χ}_{npm}, can be made from a variety of np pairs. However it is also due in part to the fact that the z-integral factors in (41) and (53) are found (by numerical integration) to vary relatively little between modes. Consequently, modes within a sub-set of modes with the same $m\chi$ and which have close to the minimum critical Rayleigh number are virtually degenerate in the sense that they contribute equally to Nu. It would matter little if some of these modes were omitted from the optimisation, so long as a few such modes are retained for each $m\chi$. The amplitudes of the retained modes merely increase as other modes are dropped, leaving Nu virtually unchanged. It was demonstrated explicitly in the numerical investigations that the optimised Nu is insensitive to the number of modes which are retained for each $m\chi$, providing there are a few modes for every active $m\chi$.

However, the factor of $(\tilde{\tau} / \tau)^2$ in the second term of (53) varies substantially when the $m\chi$ and $\tilde{m}\tilde{\chi}$ modes are different. Consequently, each $m\chi$ makes a different contribution to the Nusselt number,

and hence there is a group of different, non-zero amplitudes for each $m\chi$. Each $m\chi$ group favours those np with R^{χ}_{npm} values close to the minimum for that $m\chi$. Whilst the favoured modes with the same $m\chi$ are degenerate as regards their contribution to Nu, modes with different $m\chi$ provide independent contributions to Nu with differing optimised magnitudes, as illustrated by Figure 5.

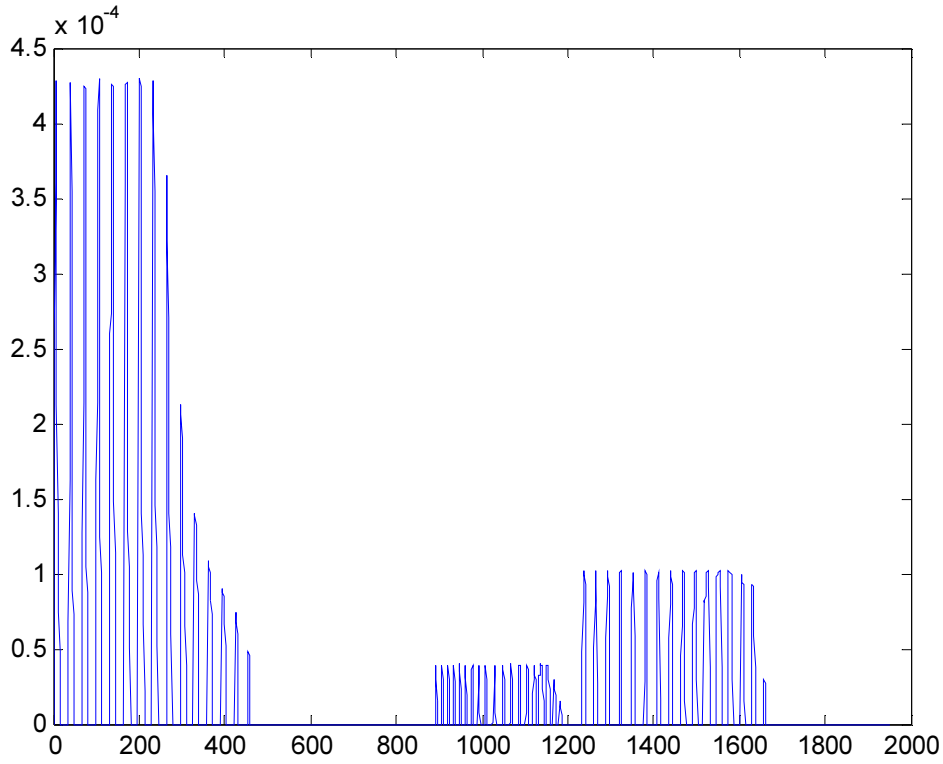

FIG. 5. Illustration of the optimised mean-squared amplitudes when all modes are retained in the optimisation ($R_a = 10^5$, $L_x = L_y = 6b$). The amplitudes plotted are $\left\langle \left(\Omega^{\chi}_{npm}\right)^2 \right\rangle_t = \left\langle \left(\tilde{\Omega}^{\chi}_{npm}\right)^2 \right\rangle_t / (k\tau)^2$. The *x*-axis is the mode number (defined in the text), there being 1950 contributing modes.

The insensitivity of the optimised Nu to the number of modes retained for each $m\chi$ is rather fortunate since otherwise the optimisation problem would have been prohibitively computationally heavy for large R_a. The complete set of modes was retained for R_a up to 10^5. But it was found that for $R_a = 10^5$ and $L_x = L_y = 6b$ the optimised Nusselt number obtained by retaining all 1950 modes differed negligibly from that obtained using just three modes, i.e., one for each different $m\chi$. For a Rayleigh number of 10^9 and $L_x = L_y = 9b$ there are 5,360,202 active modes. Had all these modes been retained the optimisation would have been most problematical. However, using just 204 modes, six per $m\chi$, gives a very reasonable result, and Nu is essentially converged using just 884 modes (26 per $m\chi$). With this number of degrees of freedom the optimisation is computationally light.

Note that all the retained modes had R^{χ}_{npm} close to the minimum for the given $pm\chi$. Retaining (say) 11 modes per $m\chi$ meant choosing arbitrarily 11 p values, the n value of the retained mode being

that which minimised R_{npm}^{χ} for that $pm\chi$. The crucial feature is that all active $m\chi$ be represented. Denoting by N_m^{χ} the number of active $m\chi$ values, retaining ζ different p values means using ζN_m^{χ} modes in all to carry out the optimisation. Values of ζ from 1 to 41 were used to demonstrate convergence. Most results were obtained for $L_x = L_y = 6b$, because this was anticipated to be sufficiently large an aspect ratio to differ negligibly from the infinite case. To demonstrate this, $L_x = L_y = 9b$ was also used and shown to result in no significant difference as regards the optimised Nu.

Figure 6 plots the total number of active modes, N, versus R_a; Figure 7 plots our optimised Nusselt number, Nu, against R_a; Figure 8 plots Nu against N; Figure 9 plots Nu against the number of active $m\chi$, N_m^{χ}; and finally Figure 10 plots Nu against the average number of active n values (which equals the average number of active p values), defined by $N_n = N_p = \sqrt{N / N_m^{\chi}}$. These five graphs reveal the following consistent set of power-law dependencies in the chaotic regime (for roughly $R_a \geq 10^5$) for the maximised Nusselt number,

$$N \propto R_a^{0.75} \qquad Nu \propto R_a^{0.25} \qquad Nu \propto N^{0.33} \qquad Nu \approx N_m^{\chi} \tag{55}$$

$$N_m^{\chi} \propto R_a^{0.25} \qquad N_n \propto R_a^{0.25} \qquad Nu \propto N_n$$

In particular, our maximised Nusselt number is roughly equal to the number of different $m\chi$ which are active, N_m^{χ}. These predictions are compared with experimental data in Section 7.

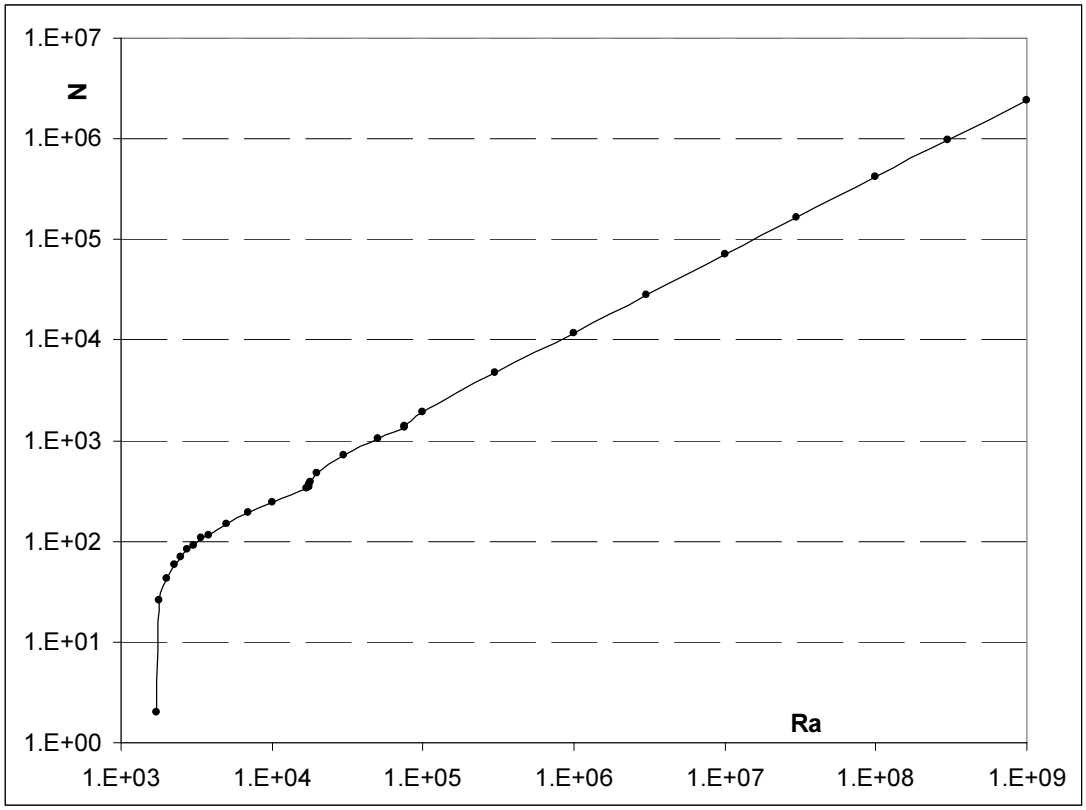

FIG. 6. Total Number of Active Modes, N , versus R_a ($L_x = L_y = 6b$)

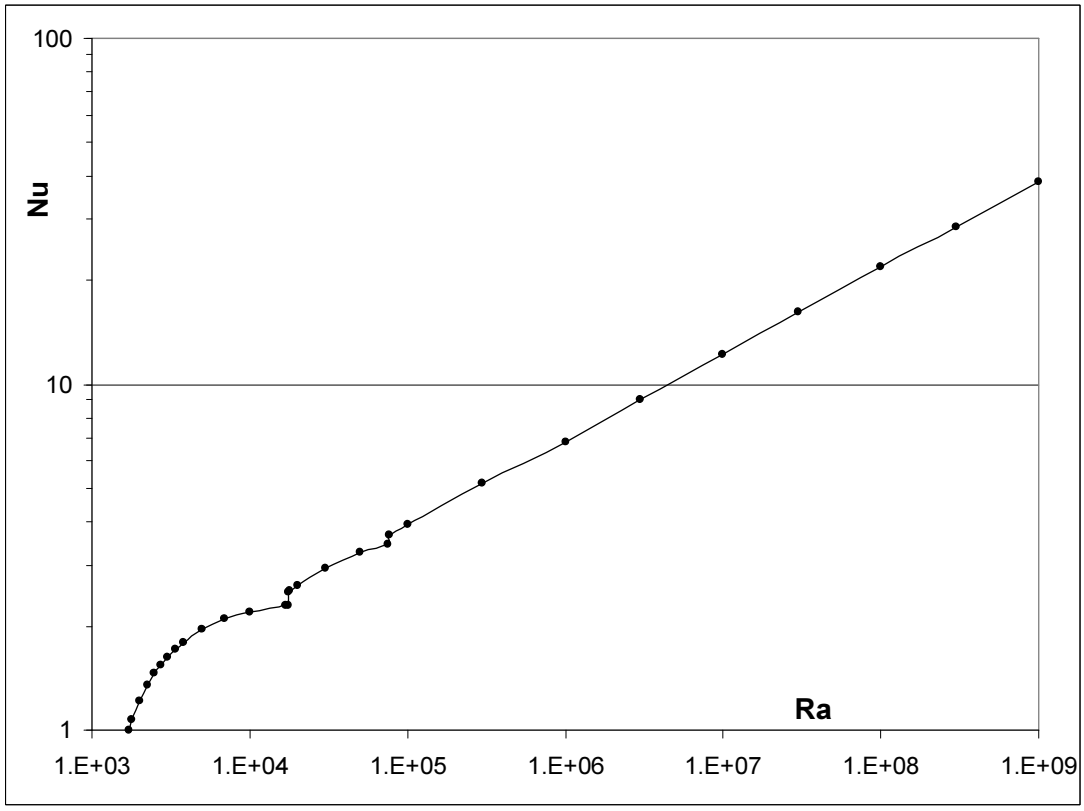

FIG. 7. Optimised Nusselt number, Nu , versus R_a

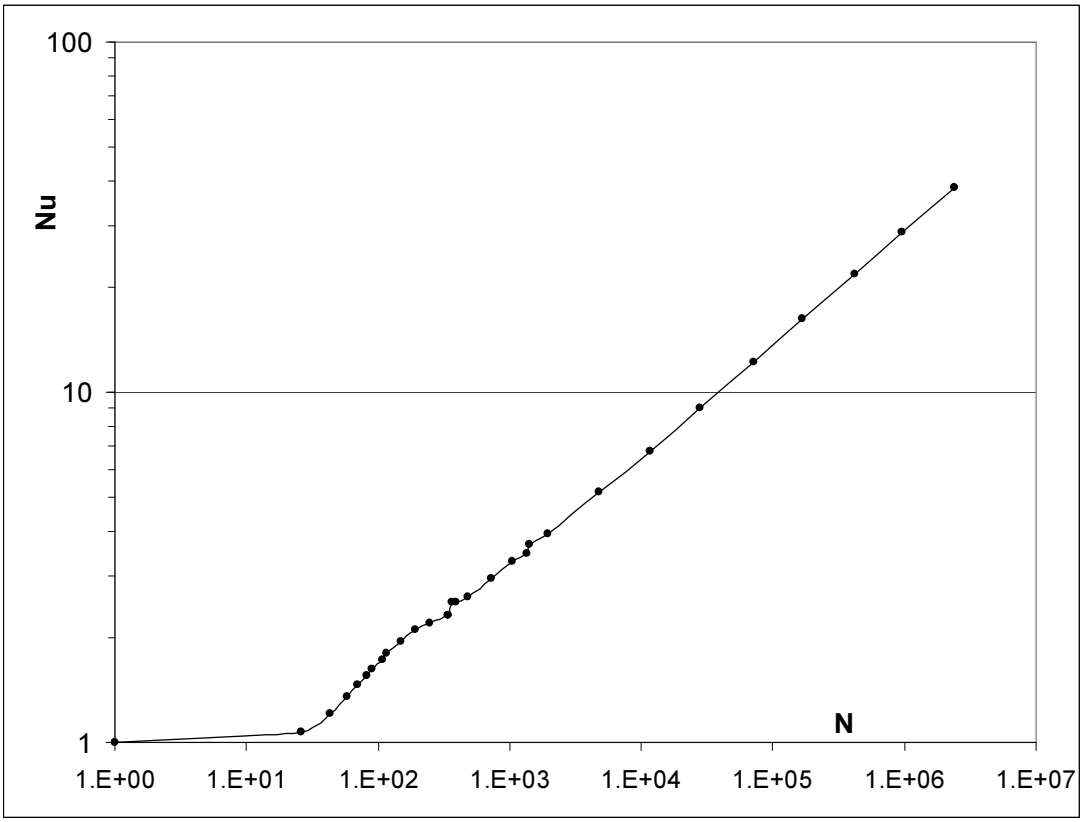

FIG. 8. Optimised Nu versus the Number of Active Modes N ($L_x = L_y = 6b$)

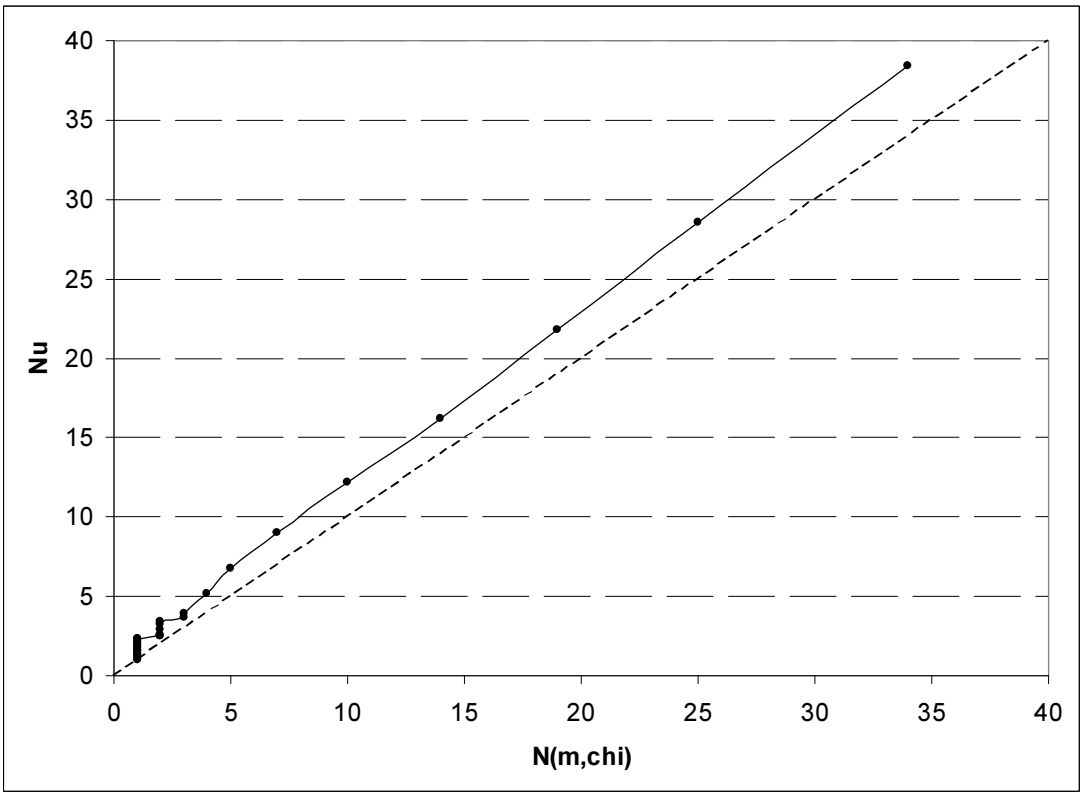

FIG. 9. Optimised Nu versus the Number of Active $m\chi$ Values, N_m^χ ; Dashed line is line of equality: $Nu = N_m^\chi$

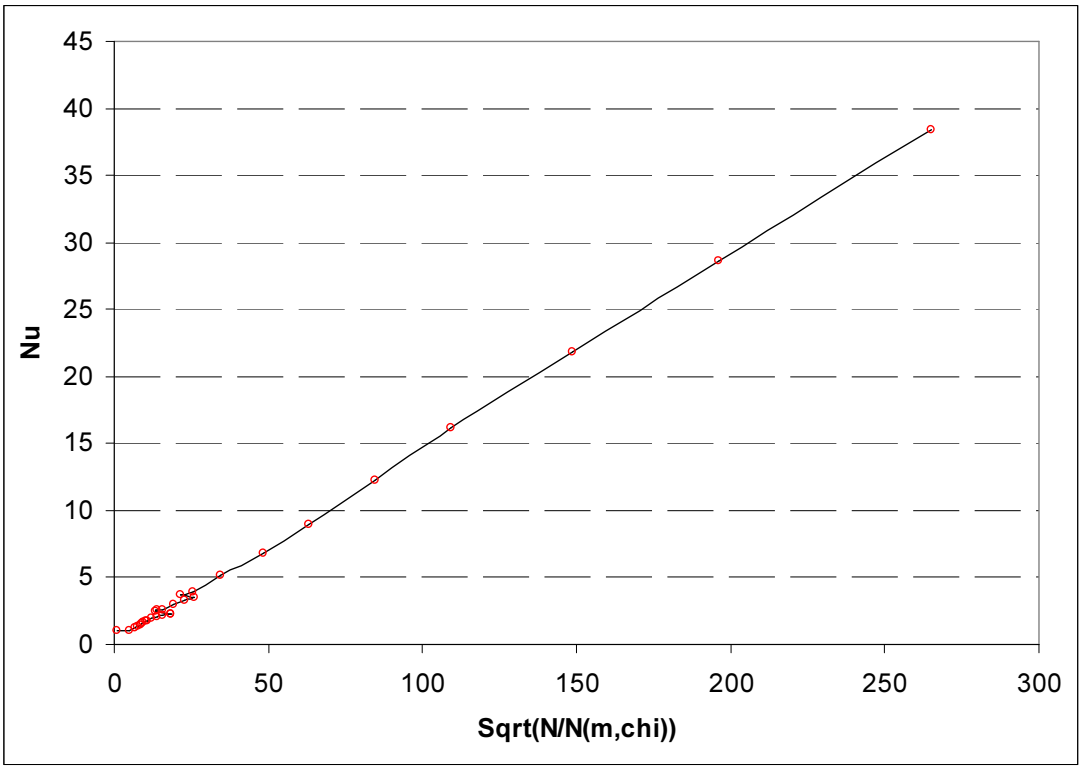

FIG.10. Optimised Nu versus the Average Number of Active n modes, $N_n = \sqrt{N / N_m^{\chi}}$ ($L_x = L_y = 6b$)

7. The Nusselt Number for a Single Mode

For a single mode, i.e., in the pre-chaotic phase, there is no optimisation to be done and a deterministic answer for Nu results. The first three terms in (53) are zero and, introducing the shorthand $\eta_{npm}^{\chi} = \left\langle \left(\omega_{npm}^{\chi} \tilde{\theta}_{npm}^{\chi} \right)^2 \right\rangle_z$, (51) and (52) give,

$$Nu = 1 + \left(\frac{1 - \dfrac{R_{npm}^{\chi}}{R_a}}{\dfrac{\eta_{npm}^{\chi}}{\left(\mu_{npm}^{\chi} \right)^2} - 1} \right) \tag{56}$$

In practice, in the single-mode regime the modes with critical Rayleigh number close to the minimum will be favoured, i.e., the $m = 1$ even modes with R_{npm}^{χ} close to 1708. Numerical evaluation of the integrals then shows that (56) reduces to,

$$Nu \approx 1 + 1.445 \left(1 - \frac{1708}{R_a} \right) \tag{57}$$

The optimised multi-mode Nu turns out to be identical to the single-mode Nu given by (57) whilst there is only one $m\chi$ active (i.e., the $m = 1$ even modes). However, the multi-mode optimised Nu exceeds (57) once the threshold of the odd modes is passed, i.e., for $R_a > 17{,}611$. The greatest single-mode, stable convection cell Nusselt number is thus 2.305.

8. Comparison with Experimental and Numerical Nusselt Number Evaluations

Comparison of the maximised Nusselt numbers obtained here with experimental and numerical evaluations in the literature will be frustrated in part by the absence of a Prandtl number dependence in the present work. The broad feature of experimental determinations of the P_r dependence of the heat transfer is that, for a given R_a, the Nusselt number has a maximum at roughly a Prandtl number of between 1 and 10. For smaller or larger Prandtl numbers, Nu reduces at fixed R_a. However the Prandtl number sensitivity of the heat transfer, whilst significant, is not dramatic. Values $P_r << 1$ or $P_r >> 1$ are required to achieve a substantial reduction in Nu. Most room-temperature liquids have $P_r > 1$, with values $P_r >> 1$ being easily achievable by using viscous liquids. Gases tend to have $0.67 < P_r < 1$, whilst liquid helium typically has Prandtl numbers in the range $0.5 < P_r \leq 0.7$. Achieving very small Prandtl numbers, $P_r << 1$, requires the use of liquid metals, generally mercury or liquid sodium, where P_r is driven to low values by their high conductivity.

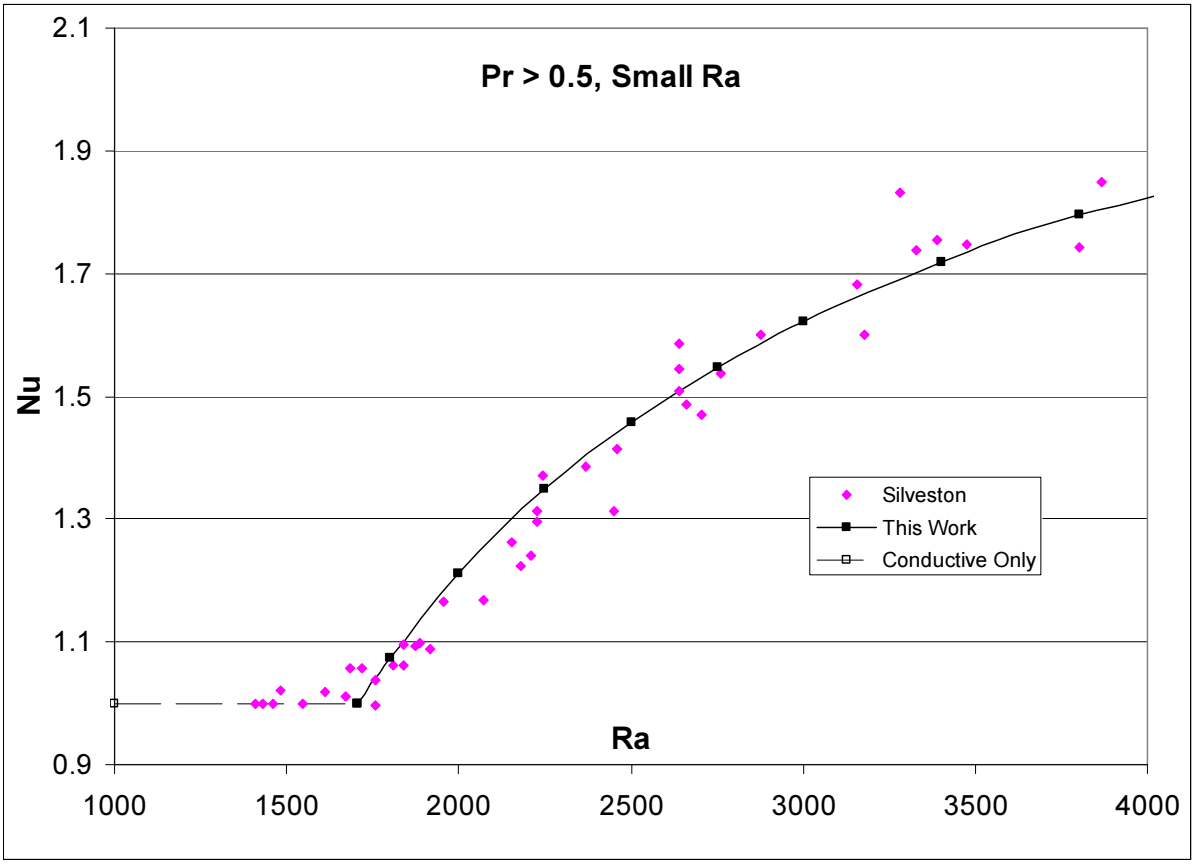

FIG. 11. Predicted and Experimental Nusselt Number Versus Rayleigh Number for Small R_a when Convection is in a Single Pure Mode (non-chaotic)

Figure 11 plots Nu against R_a in the small R_a regime when convection is in a pure mode with minimum critical Rayleigh number. The prediction, (57), is compared with the classic experimental results of Silveston [39], as quoted by Chandrasekhar [37], for a range of liquids (water, silicone oil, ethylene glycol and heptane, with P_r between 4 and 200). It is well known, of course, that the theory

for a single pure mode provides a good representation of the experimental data for sufficiently small R_a. What is new here is that if all active modes are permitted and Nu is maximised (subject to no correlations) then no increase in Nu results. Our optimised Nu values are identical to the pure-mode value given by (57) until R_a exceeds 17,611 when the first odd mode becomes active. This is a non-trivial observation: the hypothesis of maximal Nu does not undermine the agreement with experimental results in the very small R_a regime.

It is tempting to identify the activation of the lowest odd mode at $R_a > 17{,}611$ with the potential for chaotic behaviour to arise. If so, this would be something of a triumph for MEPP since this is the Rayleigh number at which maximising the heat flux implies a switch to a mixture of uncorrelated modes.

Figure 12 plots our maximised Nu against R_a in the chaotic regime up to $R_a = 10^9$ in comparison with a range of experimental evaluations for Prandtl numbers $P_r > 0.5$. These involve a range of room-temperature liquids as well as data for air, helium and liquid helium obtained from Silveston [39], Mull & Reiher [40], Turner [41], Julien et al [42], Rossby [43], Chavanne et al [44], Funfschilling et al [45] and a curve fitted to a range of experimental data in Kreith et al [46]. Other sources of experimental data could be added but these are sufficiently representative. In Figure 12 the experimental data has been replaced by an approximate trend line in most cases, to aid the comparison. The data of Silveston and of Mull and Reiher was taken from Chandrasekhar [37] and has been represented by approximate upper and lower bounds (UB and LB). A limitation of the comparison is that the experimental data of Figure 12 was obtained using a range of different aspect ratios, some quite small and hence not strictly comparable with the large aspect ratio of our calculations. However, aspect ratio dependence is believed to be relatively modest (Ahlers et al [47]).

Figure 12 shows how the experimental Nu departs from the single-mode curve at around $R_a \sim 10^4$ or just before. Our maximised Nu departs from the pure-mode curve when $R_a > 17{,}611$, when the first odd mode becomes active. A step in the curve of maximised Nu is evident at this point, Figure 12. There is a subsequent step at $R_a = 75{,}730$ when the first $m = 2$ (even) mode becomes active. Remarkably, the maximised Nu provides a good representation of the lower lying experimental data up to $R_a \sim 10^6$. Thereafter the maximised Nu starts to diverge from the experimental data. This is because the trend of the maximised Nusselt number is $Nu \propto R_a^{0.25}$, see (55) and Figure 7, whereas the experimental data for $P_r > 0.5$ commonly shows $Nu \propto R_a^{\gamma}$ with an exponent of at least $\gamma \approx 2/7$, and possibly $\gamma \approx 1/3$, even perhaps increasing to $\gamma \approx 1/2$ in the "ultimate" regime of extremely large R_a, well beyond that plotted in Figure 12 (see the reviews of Ahlers et al [47] and Manneville [48]).

However, the trend $Nu \propto R_a^{0.25}$ has theoretical precedent. For example, Ahlers et al [47] identify four regimes of behaviour according to whether boundary or bulk contributions to dissipation dominate. In the case that the boundary, including plume effects, dominates over the bulk as regards both kinetic energy and thermal dissipation rates, the arguments of Grossmann and Lohse [49] imply $Nu \propto R_a^{0.25}$. The same theory predicts the maximum behaviour of Nu as a function of P_r at fixed R_a. In particular Grossmann and Lohse [49] theory predicts Nu to reduce as $Nu \propto P_r^{\frac{1}{8}}$ as P_r is reduced in

the regime $P_r < 1$. Data for $P_r << 1$ is not as extensive as for $P_r > 0.5$. However, Figure 13 plots Nu data obtained using mercury by Cioni et al [50] and using liquid sodium by Horanyi et al [51], together with the results of numerical solutions by Verzicco and Camussi [52] and Kerr and Herring [53]. The results shown in Figure 13 relate to either $R_a = 6\times10^5$ or $R_a = 10^7$ and our corresponding maximised Nu are plotted for comparison. Nu does appear to reduce roughly as $Nu \propto P_r^{\frac{1}{8}}$. Our maximised results lie within the range of the experimental and computational data, but cannot reproduce the P_r dependence.

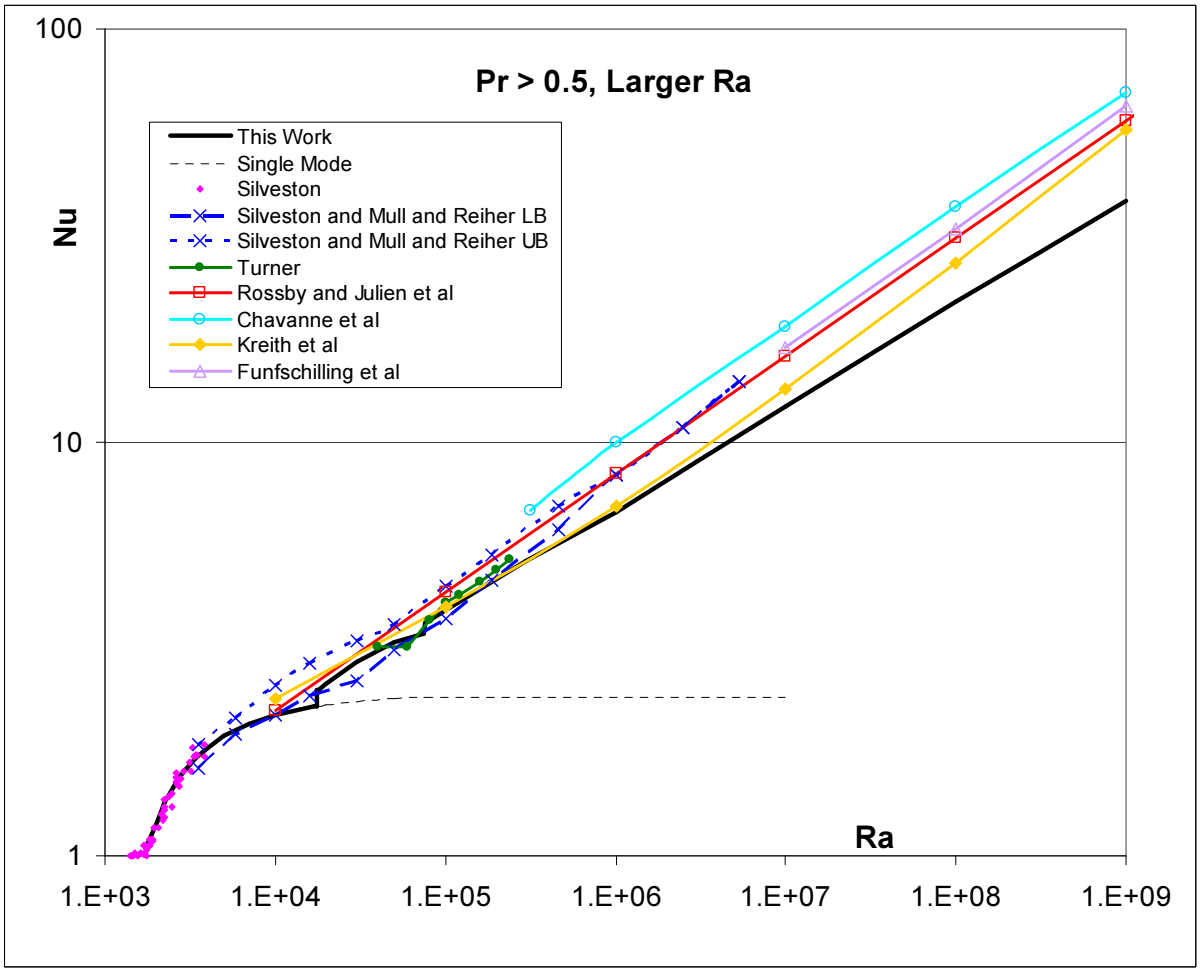

FIG. 12. Comparison of the Maximised Nusselt Numbers with Experimental Values and Extending into the Chaotic and Turbulent Regimes (experimental data for $P_r > 0.5$)

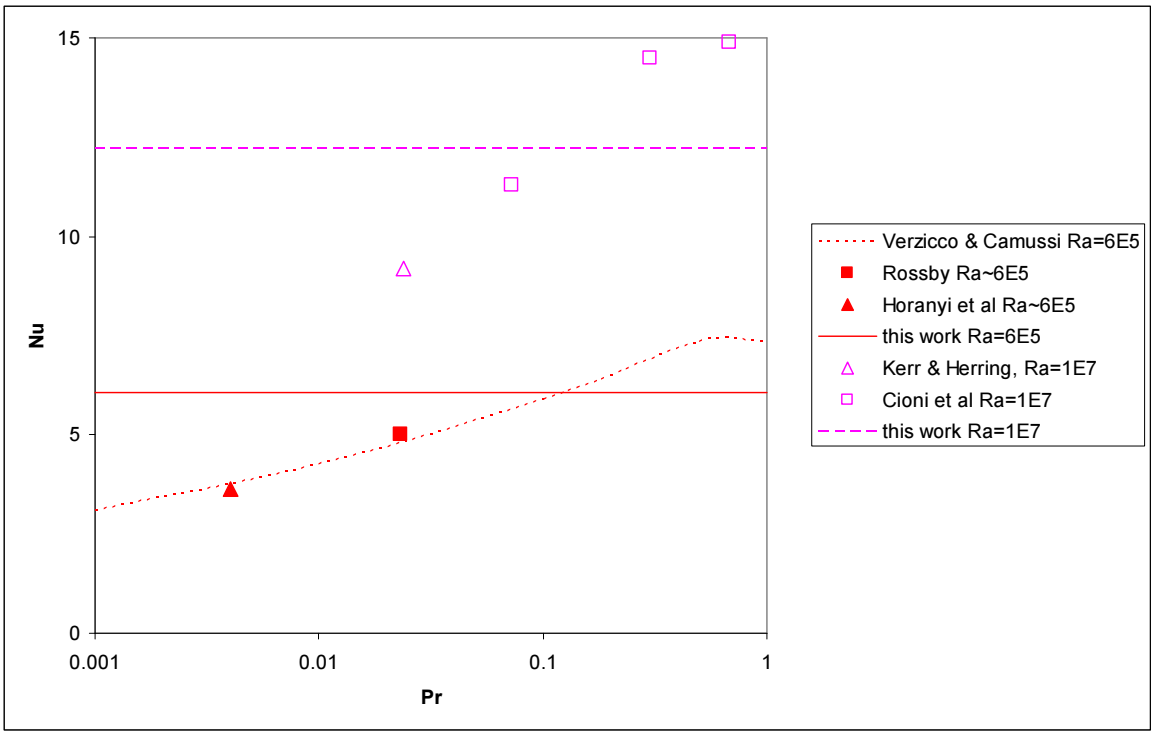

FIG. 13. Maximised Nu Compared With Experimental (Liquid Metal) and Numerical Results Obtained for $P_r << 1$

9. Discussion and Conclusions

The agreement between the maximised Nusselt numbers derived here and the experimental and numerical results in the literature, as shown in Figures 12 and 13, is reasonably good, given that this is inevitably limited by the absence of a Prandtl number dependence in the former. That the maximised Nu should be even crudely of the right order of magnitude is not immediately obvious. Indeed the wildly excessive maximised Nusselt number which can result by contriving correlations between modes emphasises the non-trivial nature of the result when correlations are assumed to be zero. Recall that these results have been obtained without any appeal to the dynamics (the Navier-Stokes equation), except through the marginally stable modes and their critical Rayleigh numbers.

An unlooked-for outcome of the present work is that, if MEPP is indicative, the Nusselt number is simply related to the mode statistics, either the total number of active modes (Figure 8), or the number of distinct active vertical mode $m\chi$ values (Figure 9), or the average number of active horizontal modes (Figure 10), these being expressed by $Nu \propto N^{0.33}$, $Nu \approx N_m^{\chi}$ and $Nu \propto N_n$ respectively. The most surprising is the (admittedly crude) approximate equality of the Nusselt number and the number of distinct active vertical mode $m\chi$ values, $Nu \approx N_m^{\chi}$. But this is limited to modest Rayleigh numbers for which $Nu \propto R_a^{0.25}$ does not depart too much from reality.

Two reactions to these results are possible. The first is that the reasonable results obtained by maximising Nu are just fluke and have no fundamental significance. The second is that there is indeed a fundamental basis for variational principles of this kind. Discrimination between these two possibilities will require the performance of MEPP to be assessed across a number of different problems. The present results suggest that there are reasons to be optimistic that MEPP does provide a reasonable, if approximate, guide to the dynamic steady states of non-equilibrium systems.

Appendix: Derivation of Equ.(38)

The derivation requires (1) and (3) but not (2). In the steady state $\langle \partial_t T \rangle_t = 0$ and so (1) gives,

$$\langle \overline{u} \cdot \overline{\nabla} T \rangle_t = \kappa \langle \nabla^2 T \rangle_t = \kappa \nabla^2 \langle T \rangle_t \tag{A1}$$

where we have appealed to the spatial derivative commuting with the time integral. Taking the x,y average of (A1) gives,

$$\langle \overline{u} \cdot \overline{\nabla} T \rangle_{txy} = \kappa \langle \nabla^2 \langle T \rangle_t \rangle_{xy} \tag{A2}$$

Alternatively we may retain the time dependence by taking the x,y average of (1) to give,

$$\left(\langle \overline{u} \cdot \overline{\nabla} T \rangle_{xy} + \partial_t \widetilde{T}_0 \right) = \kappa \langle \nabla^2 T \rangle_{xy} \tag{A3}$$

Consider the first term on the RHS of (A3),

$$\langle \partial_x^2 T \rangle_{xy} = \langle \partial_x^2 T_1 \rangle_{xy} = \left\langle \frac{1}{L_x} \int_0^{L_x} \partial_x^2 T_1 \cdot dx \right\rangle_y = \frac{1}{L_x} \langle \partial_x T_1 \big|_0^{L_x} \rangle_y = 0 \tag{A4}$$

Where we have used the fact that the conductive heat flux in the *x* direction $J_x \propto \partial_x T = \partial_x T_1$ has to be zero on the *x*-boundaries, $x = 0$ and $x = L_x$. In the same way,

$$\langle \partial_y^2 T \rangle_{xy} = 0 \tag{A5}$$

In the last term on the RHS of (A3) we have,

$$\langle \partial_z^2 T_1 \rangle_{xy} = \partial_z^2 \langle T_1 \rangle_{xy} = 0 \tag{A6}$$

Hence,

$$\langle \partial_z^2 T \rangle_{xy} = \langle \partial_z^2 \widetilde{T}_0 \rangle_{xy} = \partial_z^2 \widetilde{T}_0 \tag{A7}$$

This is the only surviving term on the RHS of (A3). If we had considered (A2) instead it would simply be the time-average of this, i.e., $\partial_z^2 \langle \widetilde{T}_0 \rangle_t$. Now consider the LHS of (A3). Integrating the first term by parts gives,

$$\begin{aligned} \langle u_x \partial_x T \rangle_{xy} = \langle u_x \partial_x T_1 \rangle_{xy} &= \left\langle \frac{1}{L_x} \int_0^{L_x} u_x \partial_x T_1 \cdot dx \right\rangle_y = \frac{1}{L_x} \left\langle (u_x T_1)_0^{L_x} - \int_0^{L_x} T_1 \partial_x u_x \cdot dx \right\rangle_y \\ &= -\frac{1}{L_x} \left\langle \int_0^{L_x} T_1 \partial_x u_x \cdot dx \right\rangle_y = -\frac{1}{L_x L_y} \int_0^{L_x} \int_0^{L_y} T_1 \partial_x u_x \cdot dx dy \end{aligned} \tag{A8}$$

where we have used $u_x = 0$ on $x = 0$ and $x = L_x$. Using the corresponding result for $\langle u_y \partial_y T \rangle_{xy}$ and adding the two gives,

$$\begin{aligned}\left\langle u_x\partial_x T + u_y\partial_y T\right\rangle_{xy} &= -\frac{1}{L_xL_y}\int_0^{L_x}\int_0^{L_y} T_1\left(\partial_x u_x + \partial_y u_y\right)\cdot dxdy \\ &= \frac{1}{L_xL_y}\int_0^{L_x}\int_0^{L_y} T_1\partial_z u_z \cdot dxdy = \left\langle T_1\partial_z u_z\right\rangle_{xy}\end{aligned} \tag{A9}$$

where we have used $\partial_j u_j = 0$ due to incompressibility. Hence we find,

$$\begin{aligned}\left\langle u_j\partial_j T\right\rangle_{xy} &= \left\langle u_x\partial_x T + u_y\partial_y T\right\rangle_{xy} + \left\langle u_z\partial_z T\right\rangle_{xy} = \left\langle T_1\partial_z u_z\right\rangle_{xy} + \left\langle u_z\partial_z T_1\right\rangle_{xy} + \left\langle u_z\partial_z \widetilde{T}_0\right\rangle_{xy} \\ &= \partial_z\left\langle u_z T_1\right\rangle_{xy}\end{aligned} \tag{A10}$$

where we have used $\left\langle u_z\partial_z \widetilde{T}_0\right\rangle_{xy} = \partial_z \widetilde{T}_0\left\langle u_z\right\rangle_{xy} = 0$, which appeals to the average velocity over a horizontal plane being zero in the steady state (because there can be no net flux of mass across such a plane and the density is constant). Hence with (A7) and (A10), (A3) becomes,

$$\partial_z\left\langle u_z T_1\right\rangle_{xy} + \partial_t \widetilde{T}_0 = \kappa\partial_z^2 \widetilde{T}_0 \tag{A11}$$

Since $\left\langle \partial_t \widetilde{T}_0\right\rangle_t = 0$ in steady state, the time-average of (A11) gives,

$$\partial_z\left\langle u_z T_1\right\rangle_{txy} = \kappa\partial_z^2\left\langle \widetilde{T}_0\right\rangle_t \tag{A12}$$

(A11) and (A12) are exact, and not dependent upon any approximations other than the Boussinesq approximation. They have been derived assuming the energy equation and incompressibility only. Integrating (A12) twice and using the boundary values of temperature on the two surfaces we get,

$$\kappa\left\langle \widetilde{T}_0(z)\right\rangle_t = \kappa T_B + \int_{-b/2}^{z}\left\langle u_z T_1\right\rangle_{txy} dz - \left\{\kappa\Delta T + \int_{-b/2}^{b/2}\left\langle u_z T_1\right\rangle_{txy} dz\right\}\left(\frac{z}{b}+\frac{1}{2}\right) \tag{A13}$$

where $\Delta T = T_B - T_T$. Recall that the boundary values of the temperature terms are $T_0 = T_B$, $T_1 = T_2 = 0$, $\widetilde{T}_0 = T_B$ on $z = -b/2$ and $T_0 = T_T$, $T_1 = T_2 = 0$, $\widetilde{T}_0 = T_T$ on $z = b/2$. (A13) obeys these boundary conditions. Note carefully the limits of the integrals in (A13). The notation on the LHS emphasises its z-dependence. Differentiating it gives,

$$\kappa\partial_z\left\langle \widetilde{T}_0\right\rangle_t = \left\langle u_z T_1\right\rangle_{txy} - \kappa\beta - \left\langle u_z T_1\right\rangle_{txyz} \tag{A14}$$

where $\beta = \Delta T / b$. Evaluating (A14) on $z = \pm b/2$ the first term on the RHS is zero and the LHS, when averaged over the x,y plane, is the average heat flux (modulo $C\rho$). Hence (A14) gives equ.(39) for the Nusselt number. We shall also need $\partial_z \widetilde{T}_0$ prior to time-averaging. Integrating (A11) twice and using the boundary values of temperature on the two surfaces we get,

$$\kappa\widetilde{T}_0 = \kappa T_B + \int_{-b/2}^{z}\left\langle u_z T_1\right\rangle_{xy} dz - \left\{\kappa\Delta T + \int_{-b/2}^{b/2}\left\langle u_z T_1\right\rangle_{xy} dz\right\}\left(\frac{z}{b}+\frac{1}{2}\right) + G(z,t) \tag{A17}$$

where,
$$G(z,t) = \int_{-b/2}^{z}\left(\int \partial_t \widetilde{T}_0 \cdot dz\right)dz - \left(\frac{z}{b}+\frac{1}{2}\right)\int_{-b/2}^{b/2}\left(\int \partial_t \widetilde{T}_0 \cdot dz\right)dz \tag{A18}$$

Differentiating (A17) with respect to z gives,

$$\kappa\partial_z\widetilde{T}_0 = \langle u_z T_1\rangle_{xy} - \kappa\beta - \langle u_z T_1\rangle_{xyz} + F(z,t) \tag{A19}$$

where,

$$F(z,t) = \partial_z G(z,t) \tag{A20}$$

Since $\langle G(z,t)\rangle_t = 0$ and $\langle F(z,t)\rangle_t = 0$, (A17) and (A19) reduce to (A13) and (A14) when the time average is taken. We wish to find an expression in T_1 and u_z only. To do so first multiply the energy equation, (1), by T_1 and average over x, y, z and use $\langle T_1\partial_t T\rangle_{txy} = 0$ to give,

$$\left\langle u_j T_1\partial_j T_1 + u_z T_1\partial_z\widetilde{T}_0\right\rangle_{txyz} = \left\langle \kappa T_1\partial_z^2\widetilde{T}_0 + \kappa T_1\nabla^2 T_1\right\rangle_{txyz} \tag{A23}$$

The first term on the LHS is zero because,

$$\int_0^{L_x}\int_0^{L_y}\int_{-b/2}^{b/2} u_j T_1\partial_j T_1\cdot dxdydz = \frac{1}{2}\int_0^{L_x}\int_0^{L_y}\int_{-b/2}^{b/2}\partial_j\left[(T_1)^2 u_j\right]\cdot dxdydz = \frac{1}{2}\oint(\widetilde{T}_1)^2 u_j\cdot dS_j = 0 \tag{A24}$$

where we have appealed to the divergence theorem, and incompressibility, $\partial_j u_j = 0$, and the fact that the normal component of flow at the boundaries is zero. The first term on the RHS of (A23) is also zero since $\left\langle T_1\partial_z^2\widetilde{T}_0\right\rangle_{xy} = \partial_z^2\widetilde{T}_0\langle T_1\rangle_{xy} = 0$. Hence (A23) reduces to,

$$\left\langle u_z T_1\partial_z\widetilde{T}_0\right\rangle_{txyz} = \left\langle\langle u_z T_1\rangle_{xy}\partial_z\widetilde{T}_0\right\rangle_{tz} = \kappa\left\langle T_1\nabla^2 T_1\right\rangle_{txyz} \tag{A25}$$

Now substitute for $\partial_z\widetilde{T}_0$ from (A19) to give,

$$\left\langle\langle u_z T_1\rangle_{xy}\left[\langle u_z T_1\rangle_{xy} - \kappa\beta - \langle u_z T_1\rangle_{xyz} + F(z,t)\right]\right\rangle_{tz} = \kappa^2\left\langle T_1\nabla^2 T_1\right\rangle_{txyz} \tag{A26}$$

Time averaging results in $\left\langle\langle u_z T_1\rangle_{xy} F(z,t)\right\rangle_t = 0$, hence re-arranging (A26) to put the quadratic terms on the LHS and the quartic terms on the RHS gives,

$$\beta\langle u_z T_1\rangle_{txyz} + \kappa\left\langle T_1\nabla^2 T_1\right\rangle_{txyz} = \frac{1}{\kappa}\left\langle\left(\langle u_z T_1\rangle_{xy}\right)^2\right\rangle_{tz} - \frac{1}{\kappa}\left\langle\left(\langle u_z T_1\rangle_{xyz}\right)^2\right\rangle_t \tag{A27}$$

which is equ.(38), as was to be proved. It reduces to Chandrasekhar [37] Appendix I, Equ.(19), in the case of a strict steady state when there are no time dependencies. However (A27) also applies in the chaotic average "steady state", the time variations due to fluctuations having implications in (A27) due to the time-averaging indicated.

References

[1] R.C. Dewar, Information theory explanation of the fluctuation theorem, maximum entropy production and self-organized criticality in non-equilibrium stationary states, J. Phys. A: Math.Gen. **36** (2003) 631.

[2] R.C. Dewar, Maximum entropy production and the fluctuation theorem, J. Phys. A: Math. Gen. **38** (2005) L371.

[3] S.A. Bruers, Discussion on maximum entropy production and information theory, J. Phys. A:

Math.Theor. **40** (2007) 7441.

[4] G. Grinstein, R. Linsker, Comments on a derivation and application of the "maximum entropy production" principle, J. Phys. A: Math. Theor. **40** (2007) 9717.

[5] R.C. Dewar, Maximum Entropy Production as an Inference Algorithm that Translates Physical Assumptions into Macroscopic Predictions: Don't Shoot the Messenger, Entropy **11** (2009) 931.

[6] N. Virgo, From maximum entropy to maximum entropy production: a new approach, Entropy **12** (2010) 107.

[7] L.M. Martyushev, V.D. Seleznev, Maximum entropy production principle in physics, chemistry and biology, Phys. Report **426** (2006) 1-45.

[8] L.M. Martyushev, The maximum entropy production principle: two basic questions, Phil. Trans. R. Soc. B **365** (2010) 1333-1334.

[9] F.J.R. Meysman, S. Bruers, Ecosystem functioning and maximum entropy production: a quantitative test of hypotheses, Phil. Trans. R. Soc. B **365** (2010) 1405–1416.

[10] R.K. Niven, Steady state of a dissipative flow-controlled system and the maximum entropy production principle, Phys. Rev. E **80** (2009) 021113.

[11] G.W. Paltridge, The steady-state format of global climate systems, Quart. J. Roy. Meteorological. Soc. **104** (1975) 927.

[12] J. Dyke, A. Kleidon, The Maximum Entropy Production Principle: Its Theoretical Foundations and Applications to the Earth System, Entropy **12** (2010) 613.

[13] R.D. Lorenz, J.I. Lunine, P.G. Withers, Titan, Mars and Earth: entropy production by latitudinal heat transport, Geophys. Res. Lett. **28** (2001) 415.

[14] S. Shimokawa, H. Ozawa, On the thermodynamics of the oceanic general circulation: irreversible transition to a state with higher rate of entropy production, Quart. J. Roy. Meteorological. Soc. **128** (2002) 2115.

[15] R.D. Lorenz, Planets, life and the production of entropy, Int. J. Astrobiol. **1** (2002) 3.

[16] D. Juretic, P. Zupanovic, Photosynthetic models with maximum entropy production in irreversible charge transfer steps, Computational Biology and Chemistry **27** (2003) 541.

[17] R.C. Dewar, D. Juretic, P. Zupanovic, The functional design of the rotary enzyme ATP synthase is consistent with maximum entropy production, Chemical Physics Letters **430** (2006) 177.

[18] R.K. Niven, Simultaneous Extrema in the Entropy Production for Steady-State Fluid Flow in Parallel Pipes, arXiv:0911.5014.

[19] W.V.R. Malkus, G. Veronis, Finite Amplitude Cellular Convection, J. Fluid. Mech. **4** (1958) 225-260.

[20] E.L. Koschmieder, Bénard Cells and Taylor Vortices, Cambridge University Press, 1993.

[21] T. Kita, Principle of Maximum Entropy Applied to Rayleigh-Bénard Convection, J. Phys. Soc. Jpn. **75** (2006) 124005 (arXiv:cond-mat/0611271).

[22] T. Kita, Entropy Change through Rayleigh-Bénard Convective Transition with Rigid Boundaries, J. Phys. Soc. Jpn. **76** (2007) 064006 (arXiv:0705.3926).

[23] E. Cafaro, A. Saluzzi, Behaviour of Bénard Convection from Non-Equilibrium Thermodynamics Point of View, Associazione Termotecnica Italiana, 50th Congresso, St.Vicent, 1995.

[24] I. Weaver, J.G. Dyke, K. Oliver, Can the principle of Maximum Entropy Production be used to predict the steady states of a Rayleigh-Bernard convective system?, in: Beyond The Second Law: Entropy Production and Non-Equilibrium Systems, New York, US, Springer (in press, 2012).

[25] P. Attard, Non-Equilibrium Thermodynamics and Statistical Mechanics: Foundations and

Applications, Chapter 6, Oxford University Press, 2012.

[26] P. Attard, Optimising Principle for Non-Equilibrium Phase Transitions and Pattern Formation with Results for Heat Convection, arXiv:1208.5105 (2012).

[27] F.H. Busse, J. Math. and Phys. **46** (1967) 140.

[28] F.H. Busse, J.A. Whitehead, Instabilities of convection rolls in a high Prandtl number fluid, J. Fluid Mech. **47** (1971) 305.

[29] L.N. Howard, Heat Transport in Turbulent Convection, J. Fluid Mech. **17** (1963) 405-432.

[30] R.A. Worthing, Contributions to the Variational Theory of Convection, PhD thesis, Michigan Technological University, 1995.

[31] F. Otto, C. Seis, Rayleigh-Bénard convection: improved bounds on the Nusselt number, J. Math. Phys. **52** (2011) 083702.

[32] J.P. Whitehead, C.R. Doering, The ultimate regime of two-dimensional Rayleigh-Bénard convection with stress-free boundaries, Phys. Rev. Lett. **106** (2011) 244501.

[33] J. Thomson, On a changing tessellated structure in certain liquids, Proc. Phil. Soc. Glasgow **13** (1882) 464.

[34] H. Bénard, Les Tourbillons cellulaires dans une nappe liquide, Revue generale des Sciences pures et appliquees **11** (1900) 1261 and 1309.

[35] H. Bénard, Les Tourbillons cellulaires dans une nappe liquide transportant de la chaleur par convection en regime permanent, Annales de Chimie et de Physique **23** (1901) 62.

[36] Lord Rayleigh, On convective currents in a horizontal layer of fluid when the higher temperature is on the under side, Phil. Mag. **32** (1916) 529.

[37] S. Chandrasekhar, Hydrodynamic and Hydromagnetic Stability, Oxford University Press, 1961.

[38] R. Krishnamurti, Some further studies on the transition to turbulent convection, J. Fluid Mech. **60** (1973) 285.

[39] P.L. Silveston, Warmedurchgang in waagerechten Flussigkeitsschichten, Part 1 Forsch. Ing. Wes. **24** (1958) 29 and 59.

[40] W. Mull, H. Reiher, Der warmeschutz von luftschichten, Gesundh-Ing. Beihefte, Reihe 1 **28** (1930) 1.

[41] J.S. Turner, Buoyancy Effects in Fluids, Cambridge University Press, 1973.

[42] K. Julien, S. Legg, J.C. McWilliams, J. Werne, Rapidly rotating turbulent Rayleigh-Bénard convection, J. Fluid Mech. **322** (1996) 243.

[43] H.T. Rossby, A study of Bénard convection with and without rotation, J. Fluid Mech. **36** (1969) 309.

[44] X. Chavanne, F. Chill, B. Castaing, B. Hebral, B. Chabaud, J. Chaussy, Observation of the ultimate regime in Rayleigh-Bénard convection, Phys. Rev. Lett. **79** (1997) 3648.

[45] D. Funfschilling, E. Brown, A. Nikolaenko, G. Ahlers, Heat transport by turbulent Rayleigh-Bénard convection in cylindrical cells with aspect ratio one and larger, J. Fluid Mech. **536** (2005) 145.

[46] F. Kreith, R.M. Manglik, M.S. Bohn, Principles of Heat Transfer, seventh ed., Cengage Learning Custom Publishing, 2010.

[47] G. Ahlers, S. Grossmann, D. Lohse, Heat transfer and large scale dynamics in turbulent Rayleigh-Bénard convection, Reviews of Modern Physics **81** (2009) 503.

[48] P. Manneville, Rayleigh-Bénard Convection: Thirty Years of Experimental, Theoretical, and Modeling Work, in: Dynamics of Spatio-Temporal Cellular Structures, Springer Tracts in

Modern Physics **207** (2006) 41.

[49] S. Grossmann, D. Lohse, Thermal convection for large Prandtl number, Phys. Rev. Lett. **86** (2001) 3316.

[50] S. Cioni, S. Ciliberto, J. Sommeria, Strongly turbulent Rayleigh-Bénard convection in mercury: Comparison with results at moderate Prandtl number, J. Fluid Mech. **335** (1997) 111.

[51] S. Horanyi, L. Krebs, U. Müller, Turbulent Rayleigh-Bénard convection in low Prandtl number fluids, Int. J. Heat Mass Transfer **42** (1999) 3983.

[52] R. Verzicco, R. Camussi, Prandtl number effects in convective turbulence, J. Fluid Mech. **383** (1999) 55.

[53] R. Kerr, J.R. Herring, Prandtl number dependence of Nusselt number in direct numerical simulations, J. Fluid Mech. **419** (2000) 325.

[54] E.N. Lorenz, Deterministic nonperiodic flow, J. Atmos. Sci. **20** (1963) 13.